

Multi-input enhanced model reference adaptive control strategies and their application to space robotic manipulators

*Original*

Multi-input enhanced model reference adaptive control strategies and their application to space robotic manipulators / Montanaro, U.; Martini, S.; Hao, Z.; Gao, Y.; Sorniotti, A.. - In: INTERNATIONAL JOURNAL OF ROBUST AND NONLINEAR CONTROL. - ISSN 1099-1239. - 33:10(2023), pp. 5246-5272. [10.1002/rnc.6639]

*Availability:*

This version is available at: 11583/2990751 since: 2024-07-13T11:56:24Z

*Publisher:*

Wiley

*Published*

DOI:10.1002/rnc.6639


*Terms of use:*

This article is made available under terms and conditions as specified in the corresponding bibliographic description in the repository

*Publisher copyright*

(Article begins on next page)

# Multi-input enhanced model reference adaptive control strategies and their application to space robotic manipulators

Umberto Montanaro<sup>1</sup>  | Simone Martini<sup>1,2</sup> | Zhou Hao<sup>3</sup> | Yang Gao<sup>4</sup> | Aldo Sorniotti<sup>1</sup>

<sup>1</sup>School of Mechanical Engineering Sciences, University of Surrey, Guildford, UK

<sup>2</sup>D. F. Ritchie School of Engineering and Computer Science, University of Denver, Denver, Colorado, USA

<sup>3</sup>Centre for Vision Speech and Signal Processing, Department of Electrical and Electronic Engineering, University of Surrey, Guildford, UK

<sup>4</sup>STAR Lab, School of Mechanical Engineering Sciences, University of Surrey, Guildford, UK

## Correspondence

Umberto Montanaro, School of Mechanical Engineering Sciences, University of Surrey, Guildford GU2 7XH, UK.

Email: [u.montanaro@surrey.ac.uk](mailto:u.montanaro@surrey.ac.uk)

## Abstract

The Enhanced Model Reference Adaptive Control (EMRAC) algorithm, augmenting the MRAC strategy with adaptive integral and adaptive switching control actions, is an effective solution to impose reference dynamics to plants affected by parameter uncertainties, unmodeled dynamics and disturbances. However, the design of the EMRAC solutions has so far been limited to single-input systems. To cover the gap, this paper presents two extensions of EMRAC to multi-input systems. The adaptive mechanism of both solutions includes the  $\sigma$ -modification strategy to assure the boundedness of the adaptive gains also in presence of persistent disturbances. The closed-loop system is analytically studied, and conditions for the asymptotic convergence of the tracking error are presented. Furthermore, when the plant is subjected to unmatched disturbances, the ultimate boundedness of the closed-loop dynamics, which are made discontinuous by the adaptive switching control actions, is systematically proven by using Lyapunov theory for Filippov systems. The problem of trajectory tracking for space robotic arms in presence of unknown and noncooperative targets is used to test the effectiveness of the novel multi-input EMRAC algorithms for taming uncertain systems. Four EMRAC solutions are designed for this engineering application, and tested within a high fidelity simulation framework based on the Robot Operating System. Finally, the tracking performance of the EMRAC implementations is quantitatively evaluated via a set of key performance indicators in the joint space and operational space, and compared with that of four benchmarking controllers.

## KEYWORDS

control of robotic arms for space applications, mechatronic, model reference adaptive control, nonlinear control

## 1 | INTRODUCTION

Model reference adaptive control (MRAC) is an effective control design method for imposing the dynamics of a reference model to plants with uncertain parameters. An established theoretical framework supports this control approach, which, over the past decades, has been shown to be a viable solution to control engineering plants with unknown parameters.<sup>1,2</sup> Nowadays, MRAC research focuses on improving the closed-loop performance of the original algorithms (e.g., by combining MRAC with other control techniques such as sliding mode control,<sup>3</sup> iterative learning control<sup>4</sup> or fuzzy algorithms,<sup>5</sup> just to name a few) and further extend the MRAC theory, for example, to fractional order systems,<sup>6</sup> switching control systems,<sup>7,8</sup> and piecewise affine systems.<sup>9-11</sup>

To improve the closed-loop tracking performance in presence of plant parameter mismatches, unmodeled plant dynamics, rapid varying disturbances, and unknown system nonlinearities, in Reference 12 the MRAC strategy was augmented by an adaptive integral control action and an adaptive switching control action. Since then, the MRAC algorithm equipped with these additional adaptive control actions, also known in the literature as Enhanced MRAC (EMRAC),<sup>13</sup> has been shown to be an effective solution for steering the dynamics of engineering plants affected by disturbances and model uncertainties toward those of a reference model. Examples of applications where the EMRAC has been successfully implemented include electronic throttle valves,<sup>12</sup> common rail systems,<sup>14</sup> thermo-hygrometric control for multi-enclosed thermal zones,<sup>15</sup> and path tracking control for autonomous vehicles.<sup>16</sup> Furthermore, in Reference 17 a discrete-time version of the EMRAC algorithm was proposed, and it was shown experimentally that the adaptive integral and switching control actions are crucial for improving the tracking of the reference dynamics, compared to other robust adaptive solutions and classical MRAC techniques.

However, the EMRAC algorithms available in the literature are limited to single-input systems, which is a severe limitation of the current EMRAC theory to real systems characterized by multiple inputs. Hence, this paper aims to fill in this gap in the literature by proposing multi-input EMRAC strategies. Specifically, two multi-input EMRAC algorithms are designed and investigated. These solutions differ in the formulation of the multi-input adaptive switching control action. A first formulation for the adaptive switching control action is based on the unit vector (UV) of the closed-loop tracking error and is named EMRAC-UV, while the second one considers each component of the tracking error by using an element-wise (EW) approach, and the resulting algorithm is denoted as EMRAC-EW. Furthermore, the adaptive mechanism for the gains of the switching control action of the novel multi-input EMRAC solutions generalizes and extends that of the single-input EMRAC, while guaranteeing also the limitation of the switching adaptive gains and their first derivative.

To prevent the onset of unbounded adaptive gains in the presence of external disturbances and unmodeled dynamics, which can degrade the closed-loop tracking performance and lead to instability,<sup>18</sup> the adaptive laws of the proposed multi-input EMRAC algorithms are equipped with the  $\sigma$ -modification strategy to systematically limit the growth of the adaptive gains to persistent disturbances (i.e., disturbances belonging to  $\mathcal{L}_\infty$ ).

The closed-loop system is systematically analyzed, and the closed-loop error dynamics are proven to be globally uniformly ultimately bounded also in presence of unmatched persistent disturbances, and the ultimate bound is provided. Furthermore, as the EMRAC switching control action makes the closed-loop system nonsmooth, it is not possible to use results available in the non-linear control theory for Lipschitz vector fields,<sup>19</sup> and thus the extensions of Lyapunov theory to Filippov systems presented in Reference 20 are used for proving the closed-loop ultimate boundedness. Moreover, conditions for guaranteeing the asymptotic tracking of the reference model are also presented.

To confirm the effectiveness of the novel multi-input EMRAC algorithms to control the dynamics of challenging multi-input engineering plants, four EMRAC solutions are designed for the path tracking control of robotic arms in the space sector. Specifically, the EMRAC-UV and EMRAC-EW strategies have been implemented with and without feedback linearization (FL) techniques, which are commonly adopted in robotics for compensating nominal system nonlinearities.

The nascent space robotics industry has been strongly demanding on-orbit servicing. On-orbit servicing particularly focuses on using robotic arms sitting on spacecrafts to carry out manipulations and services for the potential targets in space. These targets can be identified as cooperative and non-cooperative, while the service spacecraft are usually classified as free-floating or free-flying.<sup>21,22</sup>

The target is said to be cooperative when it can communicate and be controlled in attitude and orbit to cooperate with the service mission; on the contrary, a target is noncooperative when it has no ability to be controlled during the service mission.<sup>23</sup>

In the case of a free-floating spacecraft, the attitude of the spacecraft platform remains uncontrolled during the manipulation, while the platform attitude is actively controlled in the case of a free-flying spacecraft. The best example is

represented by the Canadarms on the International Space Station (ISS), where the attitude of the ISS is automatically managed to compensate the impact on the ISS dynamics caused by the operation of the robot arm.

The objectives of on-orbit services include the removal of malfunctioning spacecrafts, refueling, deorbiting, and in-space manufacturing. The services are usually achieved by executing three control tasks in sequence, that is, premanipulation, grasp/capture and postcapture manipulation.<sup>24-26</sup> To date, a good amount of research in space robotic manipulation has been carried out to address the approaching, premanipulation, and grasping/capturing phases. These studies cover the control and planning of space robotic systems, and address nonlinearities and nonholonomic planning problems, as well as impedance and grasping/capturing control for both cooperative and noncooperative targets.<sup>23,27,28</sup> For the postcapturing phase, accurate trajectory tracking is critical for mission safety and servicing performance. However, the robust manipulation and control of noncooperative targets during the postcapturing phase are still challenges that limit the operating capability and range of the potential space applications. Path tracking control for noncooperative targets poses a formidable control engineering challenge, due to the unknown inertial properties and dynamics of the targets, and the noncontrollable but still active Spacecraft Attitude and Orbit Control Systems (AOCS) of the targets, which can significantly reduce the tracking accuracy of the space robotic arm.

Although adaptive control algorithms and MRAC strategies are effective solutions for control plants with parameter mismatches, and have been successfully applied to robotic arms for terrestrial applications (for instance, see the recent survey<sup>29</sup>), to the best of the authors' knowledge, in the context of space applications, only few studies tried to address the post-capturing trajectory tracking challenge for noncooperative missions by including some level of adaptation in the control strategy. For instance, to counteract the unknown mass and inertia properties of the target, an adaptive reactionless motion controller with a nonlinear regressor was proposed in Reference 30, while a control solution exploiting an RLS-based algorithm for identifying the inertia parameters of the target was suggested in Reference 31. However, the MRAC theory for the design of path tracking control solutions for noncooperative targets for space applications has not been explored yet. Hence, in this paper four multi-input EMRAC solutions are devised to tackle the trajectory tracking control problem during the postcapturing phase for unknown and noncooperative targets for single space robotic arm systems with a large attitude-controlled servicing spacecraft. Thus, for this case study, it is assumed that the target has unknown inertial properties and its AOCS autonomously counteracts the motion that the robotic arm tries to impose after the docking/connecting or grasping phase, thus generating a reaction force that acts as a disturbance on the robotic arm dynamics.

For testing the effectiveness of the four EMRAC solutions, the EMRAC controllers have been compiled as a C++ code and deployed within a real-time Robot Operating System (ROS) environment, with the simulations being carried out through the state-of-the-art Gazebo dynamic simulator. The use of the industrial-standardized ROS framework can help to efficiently and quickly implement controllers directly on real robots, and also shows the capability of the multi-input EMRAC algorithms to run in real-time, despite the two additional adaptive control actions compared to the MRAC solutions from the literature.<sup>2</sup> Furthermore, the ROS-based framework is also used to show that the four EMRAC solutions outperform four benchmark controllers with fixed gains.

The contributions of this paper are summarized as follows.

- To extend the EMRAC theory to multi-input systems through the design of two multi-input EMRAC strategies, along with a systematic analysis of the closed-loop system by using extensions of Lyapunov theory to Filippov systems.
- To propose four multi-input EMRAC solutions to tackle the trajectory tracking control problem for space manipulators operating in a free-flying mode for a noncooperative scenario during the postcapturing phase, and to test them in a ROS based simulation environment. Due to the high risk of manipulating an unknown and noncooperative target in space, the space industry and the blooming in-orbit servicing market only focus on the in-orbit servicing of communicable and healthy satellites. This study discusses the potential robust trajectory tracking solution for inertia-changed and noncooperative targets. This can greatly increase the servicing quality and expand the number of servable spacecrafts.
- To quantitatively compare the performance of the four proposed EMRAC solutions with four benchmarking feedback controllers, including a proportional integral derivative (PID) controller embedded in ROS and three full-state FL-based strategies, augmented either with a proportional integral (PI) controller, a proportional derivative (PD) controller, or a robust strategy. The comparison is carried out via a set of key performance indicators (KPIs) in the joint space and operational space.

In the remainder,  $I_n$  denotes the identity matrix in  $\mathbb{R}^{n \times n}$ , while  $\mathcal{O}_{n,m}$  is the zero matrix in  $\mathbb{R}^{n \times m}$ . Given a symmetric matrix  $\mathcal{H} \in \mathbb{R}^{n \times n}$ , then  $\lambda_{\min}(\mathcal{H})$  and  $\lambda_{\max}(\mathcal{H})$  denote the minimum and maximum eigenvalues of  $\mathcal{H}$ , respectively.

Moreover, for a sequence of matrices  $\mathcal{H}_j \in \mathbb{R}^{n_j \times n_j}$ , with  $j = 1, \dots, m$ ,  $\Delta(\mathcal{H}_1, \mathcal{H}_2, \dots, \mathcal{H}_m)$  denotes the block diagonal matrix in  $\mathbb{R}^{(n_1 + \dots + n_m) \times (n_1 + \dots + n_m)}$  with the  $j$ th diagonal block being  $\mathcal{H}_j$ .

The paper is organized as follows. Section 2 presents the novel multi-input EMRAC algorithms, that is, the EMRAC-UV and EMRAC-EW strategies, while the main theoretical results established therein are proved in Section 3. Section 4 presents EMRAC solutions for trajectory tracking control for space manipulators. Simulation results and the quantitative comparison of the closed-loop tracking performance are presented in Section 5. Finally, conclusions are drawn in Section 6, while Appendix A and Appendix B, respectively, provide the mathematical background on Filippov systems, used to prove the ultimate boundedness of the closed-loop tracking error, and details of the ROS simulation framework for the simulation analysis.

## 2 | EMRAC STRATEGIES FOR MULTI-INPUT SYSTEMS

Consider a multi-input plant of the form

$$\dot{x} = Ax + Bu + Ed + \mathcal{G}, \quad x(t_0) \in \mathbb{R}^{n_x}, \quad (1)$$

where  $x \in \mathbb{R}^{n_x}$  is the state vector of the plant,  $u \in \mathbb{R}^{n_u}$  is the plant input vector,  $n_x$  and  $n_u$  are the dimensions of the state space and control input, respectively, and  $t_0 \in \mathbb{R}$  is the initial time instant. System (1) is subjected to two types of disturbances, that is, the measurable disturbance  $d \in \mathbb{R}^{n_d}$ , with  $n_d$  being the dimension of the space of the measurable disturbance, and the nonmeasurable disturbance  $\mathcal{G} \in \mathbb{R}^{n_x}$ . Both disturbances are assumed to be bounded (i.e., there exist two constants  $\mathcal{G}_\infty > 0$  and  $d_\infty > 0$ , such that  $\|\mathcal{G}(t)\| \leq \mathcal{G}_\infty$  and  $\|d(t)\| \leq d_\infty, \forall t \geq t_0$ ). Moreover,  $A \in \mathbb{R}^{n_x \times n_x}$ ,  $B \in \mathbb{R}^{n_x \times n_u}$ , and  $E \in \mathbb{R}^{n_x \times n_d}$  are the dynamic matrix, the input matrix and the matrix of the measurable disturbance, respectively, which are assumed constant with unknown entries.

The control objective for the EMRAC is to steer the dynamics of system (1) toward those of a linear reference system while guaranteeing the boundedness of all closed-loop signals. The reference model dynamics are given by an asymptotically stable LTI system of the form

$$\dot{x}_m = A_m x_m + B_m r + E_m d, \quad (2)$$

where  $x_m \in \mathbb{R}^{n_x}$  is the reference model state,  $r \in \mathbb{R}^{n_u}$  is the reference input assumed to be bounded, while  $A_m \in \mathbb{R}^{n_x \times n_x}$ ,  $B_m \in \mathbb{R}^{n_x \times n_u}$ , and  $E_m \in \mathbb{R}^{n_x \times n_d}$  are the dynamics matrix, the input matrix, and the disturbance matrix of the reference model, respectively, with  $A_m$  being a Hurwitz matrix.

It is assumed that there exist some constant matrices  $\hat{\Phi}_R \in \mathbb{R}^{n_u \times n_u}$ ,  $\hat{\Phi}_X \in \mathbb{R}^{n_u \times n_x}$ ,  $\hat{\Phi}_D \in \mathbb{R}^{n_u \times n_d}$ , and an invertible matrix  $S \in \mathbb{R}^{n_u \times n_u}$  such that following matching conditions are satisfied

$$B_m = B\hat{\Phi}_R, \quad A_m = A + B\hat{\Phi}_X = A + B_m\hat{\Phi}_R^{-1}\hat{\Phi}_X, \quad E_m = E + B\hat{\Phi}_D = A + B_m\hat{\Phi}_R^{-1}\hat{\Phi}_D, \quad P_\phi = \hat{\Phi}_R S = S^T \hat{\Phi}_R^T > 0. \quad (3)$$

The ideal gains  $\hat{\Phi}_R$ ,  $\hat{\Phi}_X$ , and  $\hat{\Phi}_D$  can be collected in the matrix  $\hat{\Phi} \in \mathbb{R}^{n_u \times n_w}$ , with  $n_w = 2n_x + n_u + n_d$ , and in the vector  $\hat{\phi} \in \mathbb{R}^{n_u n_w}$  defined as

$$\begin{aligned} \hat{\Phi} &= \begin{bmatrix} \hat{\Phi}_X & \hat{\Phi}_R & \hat{\Phi}_D & \hat{\Phi}_I \end{bmatrix} = \begin{bmatrix} B^\dagger B_m & B^\dagger (A_m - A) & B^\dagger (E_m - E) & \mathcal{O}_{n_u, n_x} \end{bmatrix} \\ &= \begin{bmatrix} \hat{\phi}_1 & \hat{\phi}_2 & \dots & \hat{\phi}_{n_w-1} & \hat{\phi}_{n_w} \end{bmatrix}, \end{aligned} \quad (4)$$

$$\hat{\phi} = \begin{bmatrix} \hat{\phi}_1^T & \hat{\phi}_2^T & \dots & \hat{\phi}_{n_w-1}^T & \hat{\phi}_{n_w}^T \end{bmatrix}^T, \quad \text{and} \quad \|\hat{\phi}\| \leq M_\phi, \quad (5)$$

where  $\hat{\Phi}_I = \mathcal{O}_{n_u, n_x}$ ,  $\hat{\phi}_j, j = 1, 2, \dots, n_w$ , is the  $j$ th column of  $\hat{\Phi}$  and  $M_\phi$  is a known upper bound of  $\|\hat{\phi}\|$ .

The disturbance  $\mathcal{G}$  is parameterized as

$$\mathcal{G} = B_m \delta + \hat{\mathcal{G}}, \quad (6)$$

where both  $\delta \in \mathbb{R}^{n_u \times n_u}$  and  $\hat{\mathcal{G}}$  are assumed to be bounded, that is, there exist two constants  $\delta_\infty > 0$  and  $\hat{\mathcal{G}}_\infty > 0$ , such that  $\|\delta(t)\| \leq \delta_\infty$  and  $\|\hat{\mathcal{G}}(t)\| \leq \hat{\mathcal{G}}_\infty, \forall t \geq t_0$ .

The control action provided by the EMRAC algorithm for the multi-input system (1) is

$$u(t) = u_{MRAC}(t) + u_D(t) + u_I(t) + u_N(t), \quad (7)$$

where

$$u_{MRAC}(t) = K_X(t)x(t) + K_R(t)r(t), \quad (8a)$$

$$u_D(t) = K_D(t)d(t), \quad (8b)$$

$$u_I(t) = K_I(t)x_I(t), \quad (8c)$$

where  $x_I \in \mathbb{R}^{n_x}$  is the integral of the tracking error whose dynamics are computed as

$$\dot{x}_I = x_e - \sigma_I (\|x_I\|) \rho_e x_I, \quad \text{and} \quad x_e = x_m - x, \quad (9)$$

where  $x_e$  is the state tracking error,  $\rho_e \in \mathbb{R}^{n_x \times n_x}$  is a positive diagonal matrix and  $\sigma_I (\|x_I\|)$  is the  $\sigma$ -modification strategy to prevent the drift of the integral of the tracking error (9) defined as

$$\sigma_I (\|x_I\|) = \begin{cases} 0 & \text{if } \|x_I\| \leq \hat{M}_I, \\ \eta_I \left( \frac{\|x_I\|}{\hat{M}_I} - 1 \right) & \text{if } \hat{M}_I < \|x_I\| \leq 2\hat{M}_I, \\ \eta_I & \text{if } \|x_I\| > 2\hat{M}_I, \end{cases} \quad (10)$$

where  $\eta_I$  and  $\hat{M}_I$  are strictly positive constants.

The adaptive gains in (8) are computed as

$$K_X = \Phi_X + S^T y_e x^T \beta_X, \quad \text{and} \quad \dot{\Phi}_X = S^T y_e x^T \alpha_X + F_X, \quad (11a)$$

$$K_R = \Phi_R + S^T y_e r^T \beta_R, \quad \text{and} \quad \dot{\Phi}_R = S^T y_e r^T \alpha_R + F_R, \quad (11b)$$

$$K_D = \Phi_D + S^T y_e d^T \beta_D, \quad \text{and} \quad \dot{\Phi}_D = S^T y_e d^T \alpha_D + F_D \quad (11c)$$

$$K_I = \Phi_I + S^T y_e x_I^T \beta_I, \quad \text{and} \quad \dot{\Phi}_I = S^T y_e x_I^T \alpha_I + F_I, \quad (11d)$$

where  $\alpha_X, \beta_X, \alpha_I, \beta_I \in \mathbb{R}^{n_x \times n_x}$ ,  $\alpha_R, \beta_R \in \mathbb{R}^{n_u \times n_u}$ , and  $\alpha_D, \beta_D \in \mathbb{R}^{n_d \times n_d}$  are strictly positive diagonal matrices and  $F_X, F_I \in \mathbb{R}^{n_u \times n_x}$ ,  $F_R \in \mathbb{R}^{n_u \times n_u}$  and  $F_D \in \mathbb{R}^{n_u \times n_d}$  are the locking strategies for preventing the unbounded evolution of the gains (11) in the presence of disturbances and unmodeled dynamics. Moreover,  $y_e \in \mathbb{R}^{n_u}$  is computed as

$$y_e = B_m^T P_e x_e, \quad \text{with } P_e \text{ being the solution of } P_e A_m + A_m^T P_e = -Q, \quad (12)$$

where  $Q \in \mathbb{R}^{n_x \times n_x}$  is a strictly positive matrix.

The integral parts of the adaptive gains in (11) can be collected in the matrix  $\Phi \in \mathbb{R}^{n_u \times n_w}$  and the vector  $\phi \in \mathbb{R}^{n_u \times n_w}$  defined as

$$\Phi = \begin{bmatrix} \Phi_X & \Phi_R & \Phi_D & \Phi_I \end{bmatrix} = \begin{bmatrix} \phi_1 & \phi_2 & \cdots & \phi_{n_w-1} & \phi_{n_w} \end{bmatrix}, \quad (13)$$

$$\phi = \begin{bmatrix} \phi_1^T & \phi_2^T & \cdots & \phi_{n_w-1}^T & \phi_{n_w}^T \end{bmatrix}^T, \quad (14)$$

where  $\phi_j, j = 1, 2, \dots, n_w$  is the  $j$ th column of the  $\Phi$ -matrix. Moreover, the leakage terms in (11) are computed as

$$F_X = -\sigma_\phi(\|\phi\|)\Phi_X\rho_X, \quad F_I = -\sigma_\phi(\|\phi\|)\Phi_I\rho_I, \quad F_R = -\sigma_\phi(\|\phi\|)\Phi_R\rho_R, \quad F_D = -\sigma_\phi(\|\phi\|)\Phi_D\rho_D, \quad (15)$$

where  $\rho_X, \rho_I \in \mathbb{R}^{n_x \times n_x}$ ,  $\rho_R \in \mathbb{R}^{n_u \times n_u}$  and  $\rho_D \in \mathbb{R}^{n_d \times n_d}$  are strictly positive diagonal matrices and  $\sigma_\phi(\|\phi\|)$  is the  $\sigma$ -modification strategy for the adaptive gains of the smooth control actions computed as

$$\sigma_\phi(\|\phi\|) = \begin{cases} 0, & \text{if } \|\phi\| \leq \hat{M}_\phi, \\ \eta_\phi \left( \frac{\|\phi\|}{\hat{M}_\phi} - 1 \right), & \text{if } \hat{M}_\phi < \|\phi\| \leq 2\hat{M}_\phi, \\ \eta_\phi, & \text{if } \|\phi\| > 2\hat{M}_\phi, \end{cases} \quad (16)$$

where  $\eta_\phi$  and  $\hat{M}_\phi$  are strictly positive constants such that

$$\hat{M}_\phi \geq \sqrt{\frac{\lambda_{\max}(\Gamma_\rho \Gamma_\alpha^{-1} \otimes P_\phi^{-1})}{\lambda_{\min}(\Gamma_\rho \Gamma_\alpha^{-1} \otimes P_\phi^{-1})}} M_\phi, \quad \text{and} \quad \eta_\phi \lambda_{\min}(\Gamma_\rho \Gamma_\alpha^{-1} \otimes P_\phi^{-1}) > \frac{3}{4} \lambda_{\min}(Q), \quad (17)$$

where  $\otimes$  is the Kronecker product and the strictly positive matrices  $\Gamma_\rho, \Gamma_\alpha \in \mathbb{R}^{n_w \times n_w}$  are defined as

$$\Gamma_\alpha = \Delta(\alpha_X, \alpha_R, \alpha_D, \alpha_I) = \text{diag}(\alpha_1, \alpha_2, \dots, \alpha_{n_w}), \quad \text{and} \quad \Gamma_\rho = \Delta(\rho_X, \rho_R, \rho_D, \rho_I) = \text{diag}(\rho_1, \rho_2, \dots, \rho_{n_w}). \quad (18)$$

The control action  $u_N(t)$  can be set either as  $u_N^{(uv)}(t)$  or  $u_N^{(ew)}(t)$  define as

$$u_N^{(uv)}(t) = K_N^{(uv)}(t) \frac{y_e}{\|y_e\|}, \quad K_N^{(uv)} = S^T \Phi_{N0}, \quad (19)$$

$$u_N^{(ew)}(t) = K_N^{(ew)}(t) \psi(y_e), \quad K_N^{(ew)} = S^T \Phi_N, \quad \psi(y_e) = \left[ \text{sgn}(y_{e1}) \quad \text{sgn}(y_{e2}) \quad \dots \quad \text{sgn}(y_{en_u}) \right]^T, \quad (20)$$

where the dynamics of the adaptive gains  $\Phi_{N0} \in \mathbb{R}$  and  $\Phi_N = \text{diag}(\Phi_{N1}, \Phi_{N2}, \dots, \Phi_{Nn_u}) \in \mathbb{R}^{n_u}$  are

$$\dot{\Phi}_{N0} = \alpha_{N0} h_0(\|y_e\|_\Omega) - \sigma_{N0}(\|\Phi_{N0}\|) \rho_{N0} \Phi_{N0}, \quad (21)$$

$$\dot{\Phi}_{Nj} = \alpha_{Nj} h_j(|y_{ej}|) - \sigma_{Nj}(\|\Phi_{Nj}\|) \rho_{Nj} \Phi_{Nj}, \quad j = 1, \dots, n_u, \quad (22)$$

where  $\|y_e\|_\Omega = y_e^T \Omega y_e$  with  $\Omega \in \mathbb{R}^{n_u \times n_u}$  being a strictly positive matrix,  $\alpha_{Nj}, \rho_{Nj}, j = 0, 1, \dots, n_u$ , are strictly positive constants, and the  $h$ -functions are defined as

$$h_0(\|y_e\|_\Omega) = \frac{\|y_e\|_\Omega^{\zeta_0}}{\xi_0 + \gamma_0 \|y_e\|_\Omega^{\zeta_0}}, \quad (23a)$$

$$h_j(|y_{ej}|) = \frac{|y_{ej}|^{\zeta_j}}{\xi_j + \gamma_j |y_{ej}|^{\zeta_j}}, \quad j = 1, \dots, n_u, \quad (23b)$$

with  $\xi_j, \gamma_j, \zeta_j, j = 0, 1, \dots, n_u$ , are strictly positive constants.

The  $\sigma$ -modification functions  $\sigma_{Nj}(\|\Phi_{Nj}\|), j = 0, 1, \dots, n_u$ , in (21) and (22) are defined as

$$\sigma_{Nj}(\|\Phi_{Nj}\|) = \begin{cases} 0, & \text{if } \|\Phi_{Nj}\| \leq \hat{M}_{Nj}, \\ \eta_{Nj} \left( \frac{\|\Phi_{Nj}\|}{\hat{M}_{Nj}} - 1 \right), & \text{if } \hat{M}_{Nj} < \|\Phi_{Nj}\| \leq 2\hat{M}_{Nj}, \\ \eta_{Nj}, & \text{if } \|\Phi_{Nj}\| > 2\hat{M}_{Nj}, \end{cases} \quad (24)$$

where  $\eta_{Nj}$  and  $\hat{M}_{Nj}, j = 0, 1, \dots, n_u$ , are strictly positive constants and

$$\hat{M}_{N0} > \frac{\delta_\infty}{\lambda_{\min}(SP_\phi^{-1}S^T)}, \quad \text{and} \quad \hat{M}_{Nj} > \frac{\delta_{j\infty}}{\tilde{c}_j}, \quad j = 1, \dots, n_u, \quad (25)$$

where  $\tilde{c}_j > 0$  is the  $j$ -entry on the diagonal of the matrix  $SP_\phi^{-1}S^T$  and  $\delta_{j\infty} > 0, j = 1, \dots, n_u$ , are constants such that  $|\delta_j| \leq \delta_{j\infty}$ .

In the rest of the paper, when the EMRAC control action (7) is equipped  $u_N = u_N^{(uv)}$  in (19), then the resulting control strategy is named EMRAC-UV (i.e., EMRAC with the  $u_N$ -term based on the unit vector in the direction of  $y_e$ ), while when  $u_N$  is set as  $u_N = u_N^{(ew)}$  in (20), the resulting strategy is referred to as EMRAC-EW (i.e., EMRAC with the  $u_N$ -term based on each entry of the vector  $y_e$ ).

Let us now define the following vectors and matrices

$$\Phi_e = \hat{\Phi} - \Phi, \quad \phi_e = \hat{\phi} - \phi, \quad \tilde{x}_e = \begin{bmatrix} x_e^T & \phi_e^T \end{bmatrix}^T \in \mathbb{R}^{n_x+n_u n_w}, \quad (26)$$

$$\tilde{P} = \Delta(P_e, \tilde{P}_\phi) \in \mathbb{R}^{(n_x+n_u n_w) \times (n_x+n_u n_w)}, \quad \text{with} \quad \tilde{P}_\phi = \Gamma_\alpha^{-1} \otimes P_\phi^{-1} \in \mathbb{R}^{n_u n_w \times n_u n_w}, \quad (27)$$

and the positive constant and functions

$$\mu_1 = \frac{3}{4} \lambda_{\min}(Q), \quad \mu_2(\tilde{\mathcal{G}}_\infty) = \frac{3\|P_e\|^2 \tilde{\mathcal{G}}_\infty^2}{\mu_1} + \mu_1(2\hat{M}_\phi + \|\hat{\phi}\|)^2, \quad \mu(\tilde{\mathcal{G}}_\infty) = \sqrt{\frac{\mu_2(\tilde{\mathcal{G}}_\infty)}{\mu_1(1-\zeta)}} \quad \text{with} \quad \zeta \in (0, 1), \quad (28)$$

where

$$\tilde{\mathcal{G}}_\infty = \begin{cases} \hat{\mathcal{G}}_\infty^2, & \text{if } \hat{\mathcal{G}}^T B_m \delta \geq 0 \quad \forall t \geq t_0, \\ \mathcal{G}_\infty^2, & \text{otherwise.} \end{cases} \quad (29)$$

Notice that when  $\hat{\mathcal{G}}^T B_m \delta > 0$ , then  $\|\hat{\mathcal{G}}(t)\| < \|\mathcal{G}(t)\|$ , thus  $\hat{\mathcal{G}}_\infty^2 < \mathcal{G}_\infty^2$  and  $\mu(\hat{\mathcal{G}}_\infty) < \mu(\mathcal{G}_\infty)$ . This condition is satisfied for instance when the reference inputs for system (2) are decoupled, thus, after a permutation of the columns of  $B_m$ , the reference input matrix can be expressed as  $B_m = [\mathcal{O}_{n_x-n_u, n_u}^T \quad B_{mc}^T]^T$ , with  $B_{mc} = \text{diag}(b_{mc,1}, b_{mc,2}, \dots, b_{mc,n_u}) \in \mathbb{R}^{n_u \times n_u}$ . Indeed, under this condition, the entries of the  $\delta$ -vector in (6) can be set as  $\delta_j = \mathcal{G}_{j+n_x-n_u}/b_{m,j}, j = 1, \dots, n_u$ , while  $\hat{\mathcal{G}} = [\mathcal{G}_1 \quad \dots \quad \mathcal{G}_{n_x-n_u} \quad 0 \quad \dots \quad 0]^T$ , thus  $\hat{\mathcal{G}}^T B_m \delta = 0, \forall t \geq t_0$ .

**Theorem 1** (EMRAC-UV). Consider system (1) and the reference model (2). Let the adaptive control action be given by (7), where  $u_N$  is set as  $u_N^{(uv)}$  in (19) and the adaptive gains computed as in (11) and (21). Then, all the closed-loop signals are bounded. Moreover,

- a (a) if  $\hat{\mathcal{G}} \neq 0$ , then the tracking error dynamics are globally uniformly ultimately bounded, and there exists a time  $\mathcal{T}$  (dependent on  $\tilde{x}_e(t_0)$ ) such that

$$\|\tilde{x}_e(t)\| \leq \sqrt{\frac{\lambda_{\max}(\tilde{P})}{\lambda_{\min}(\tilde{P})}} \mu(\tilde{\mathcal{G}}_\infty), \quad \forall t \in [t_0 + \mathcal{T}, +\infty), \quad (30)$$

where  $\tilde{P}$  and  $\mu$  are computed as in (27) and (28), respectively;

- b (b) if  $\hat{\mathcal{G}} = 0$ , the closed-loop tracking error  $x_e$  converges to zero as the time goes to infinite, that is,

$$\|x_e(t)\| \rightarrow 0 \quad \text{when} \quad t \rightarrow +\infty. \quad (31)$$

**Theorem 2.** (EMRAC-EW) Consider system (1) and the reference model (2). Let the adaptive control action be given by (7) where  $u_N$  is set as  $u_N^{(ew)}$  in (20) and the adaptive gains are computed as in (11) and (22). If the matrix  $SP_\phi^{-1}S^T$  is diagonal, then results (a) and (b) of Theorem 1 hold also for the EMRAC-EW algorithm.



As for the Minimal Control Synthesis (MCS) adaptive strategy,<sup>32</sup> Theorems 1 and 2 hold also for linear time-varying systems when the variation of the system matrices is slower than the adaptation rate of the integral part of the adaptive gains in (11). Hence, the following corollary extends the results obtained for the MCS algorithm to the multi-input EMRAC algorithm.

**Corollary 1.** *Assume that the matrices of the plant (1) are time-varying with a rate of variation such that*

$$\frac{d\hat{\Phi}}{dt} - S^T y_e w^T \Gamma_\alpha \approx -S^T y_e w^T \Gamma_\alpha, \quad (32)$$

where

$$w = \begin{bmatrix} x^T & r^T & d^T & x_I^T \end{bmatrix}^T \in \mathbb{R}^{n_w}, \quad (33)$$

then Theorems 1 and 2 still hold.

*Remarks:*

- For system (1), the measurable disturbance  $d$  models nonmanipulated plant inputs, while  $\mathcal{G}$  represents unmodeled dynamics and unmeasurable external disturbances.
- The multi-input EMRAC strategy enhances MRAC solutions with compensation of measurable disturbances<sup>2</sup> by equipping the control strategy (7) with two additional adaptive control actions, that is, the adaptive integral action  $u_I(t)$  in (8c), and the adaptive switching control action  $u_N(t)$  computed either as in (19), for the EMRAC-UV strategy, or in (20), in the case of the EMRAC-EW solution. The adaptive integral control action improves the tracking of the reference model to unmodeled biases in the plant dynamics, for example constant disturbances, while the adaptive switching control action increases the robustness of the closed-loop tracking performance with respect to rapid varying bounded disturbances.
- The additional adaptive and integral control actions of the EMRAC, that is,  $u_I(t)$  and  $u_N(t)$ , make this strategy more computational demanding with respect to traditional MRAC algorithms. However, implementations of EMRAC solutions in ROS, investigated in this paper, suggest that the two extra control actions do not jeopardize real-time implementability of EMRAC algorithms.
- For engineering control problems, nominal plant models can be used to design the reference dynamics such that conditions (3) hold. A possible approach is to select as a reference model the nominal plant model controlled via feedback control actions (e.g., LQR strategies, see References 12,33). Furthermore, the range of variations of the plant parameters and disturbances can be utilized to select the weights of the  $\sigma$ -modification.<sup>34</sup>
- As for the multi-input MRAC strategies presented in Reference 18, the assumption on the existence of the matrix  $S$  in (3) replaces the condition of the knowledge of the sign of  $\hat{\Phi}_R$  for the single-input EMRAC.<sup>33</sup> However, when considering the canonical form of the model of robotic manipulators, the matrix  $S$  can be set as the identity matrix (see also Section 4).
- Compared to classical multi-input MRAC strategies,<sup>18</sup> in addition to the adaptive switching control action and the adaptive integral control action, the EMRAC algorithm augments the integral adaptive mechanism of the adaptive gains in (11) with (i) a proportional adaptive mechanism to improve the closed-loop tracking dynamics<sup>35</sup> and (ii) a  $\sigma$ -modification strategy, which is used, together with (24), for guaranteeing the ultimate boundedness of the closed-loop tracking error dynamics in presence of unmatched disturbances and unmodeled dynamics. Furthermore, for each component of the regressor (33), there is an integral adaptive weight, a proportional adaptive weight and leakage factor, thus allowing tailoring these control parameter for each entry of the regressor based on the control application.
- The novel adaptive laws for the gains of the switching control actions, that is, (21) and (22), guarantee that the dynamics of the gains  $\Phi_{Nj}$ , with  $j = 0, 1, \dots, n_u$ , and their derivatives are bounded for any  $y_e$ -trajectory as  $h_0(\|y_e\|_\Omega)$  and  $h_j(|y_{ej}|)$  in (23) are bounded and the  $\sigma$ -modification strategy is adopted (see also Section 3.1).
- If  $n_u = 1$ , both the EMRAC-UV and the EMRAC-EW algorithms reduce to the single-input EMRAC,<sup>33</sup> thus confirming that they are consistent extensions of the EMRAC family to the multi-input case. However, by using the novel adaptive

mechanism for the switching control action in (21) and (22), when  $n_u = 1$  the ultimate bound computed as in (30) is smaller than that presented in Reference 16 for single-input systems. Furthermore, the adaptive mechanisms (21) and (22) reduce to the one presented for the single-input EMRAC by selecting  $\varsigma_j = 1$ ,  $\xi_j = 1$ ,  $\gamma_j = 0$  in (23).

### 3 | PROOF OF THE MAIN THEOREMS

The analysis of the closed-loop system is based on the Lyapunov theory for smooth and nonsmooth dynamic systems and Barbalat's lemma to prove convergence of the tracking error. In what follows, the ultimate boundedness of  $\Phi_{N0}$  and  $\Phi_N$  is first proven in Section 3.1. Then a quadratic auxiliary Lyapunov-like function is designed for the closed-loop error dynamics in Section 3.2. This Lyapunov-like function will be then used along with the theory for non-smooth dynamic systems presented in Appendix A to prove Theorem 1 and Theorem 2 (see Section 3.3, Section 3.4 and Section 3.5). Finally, the proof of Corollary 1 is presented in Section 3.6.

The proof of the ultimate-boundedness of the closed-loop error dynamics requires the following lemma.

**Lemma 1.** *The  $\sigma$ -modification strategy (15) and (16) guarantees*

$$-\sigma_\phi(\|\phi\|)\phi_e^T \left( \Gamma_\rho \Gamma_\alpha^{-1} \otimes P_\phi^{-1} \right) \phi \geq 0, \quad \forall \phi, \quad \text{and} \quad -\sigma_\phi(\|\phi\|)\phi_e^T \left( \Gamma_\rho \Gamma_\alpha^{-1} \otimes P_\phi^{-1} \right) \phi > 0, \quad \forall \|\phi\| \geq \widehat{M}_\phi. \quad (34)$$

Moreover

$$-\sigma_\phi(\|\phi\|)\phi_e^T \left( \Gamma_\rho \Gamma_\alpha^{-1} \otimes P_\phi^{-1} \right) \phi > \frac{\eta_\phi}{2} \phi_e^T \left( \Gamma_\rho \Gamma_\alpha^{-1} \otimes P_\phi^{-1} \right) \phi_e, \quad \forall \|\phi\| \geq 2\widehat{M}_\phi. \quad (35)$$

Notice that, the proof of Lemma 1 follow identically to the proof of lemma 2 in Reference 34, thus and it is omitted for the sake of brevity.

#### 3.1 | Ultimate boundedness of $\Phi_{N0}$ and $\Phi_N$

The ultimate boundedness, and thus the boundedness, of the adaptive gains  $\Phi_{Nj}, j = 0, 1, \dots, n_u$  in (21) and (22) can be proved by using the theory of smooth nonlinear dynamics systems is<sup>19</sup> as follows.

By selecting for each gain  $\Phi_{Nj}, j = 0, 1, \dots, n_u$  the functions  $V_N, W_{Na}$  and  $W_{Nb}$  as

$$V_N(\Phi_{Nj}) = W_{Na}(\Phi_{Nj}) = W_{Nb}(\Phi_{Nj}) = \frac{\Phi_{Nj}^2}{2}, \quad (36)$$

then

$$W_{Na}(\Phi_{Nj}) \leq V_N(\Phi_{Nj}) \leq W_{Nb}(\Phi_{Nj}), \quad \forall \Phi_{Nj}, \quad j = 0, 1, \dots, n_u. \quad (37)$$

As each  $h_j, j = 0, 1, \dots, n_u$  in (23) is bounded and by using the  $\sigma$ -modification functions in (24), after some algebraic manipulations the derivative of  $V_N$  can be upper-bounded as

$$\begin{aligned} \dot{V}_N &= \alpha_{Nj} h_j \Phi_{Nj} - \sigma_{Nj}(\|\Phi_{Nj}\|) \rho_{Nj} \Phi_{Nj}^2 \\ &\leq -\rho_{Nj} \eta_{Nj} (1 - \zeta_{Nj}) \Phi_{Nj}^2 - \rho_{Nj} \eta_{Nj} \zeta_{Nj} \Phi_{Nj}^2 + H_{Nj} \Phi_{Nj} \\ &\leq -W_{Nj}(\Phi_{Nj}), \quad \text{if} \quad \|\Phi_{Nj}\| \geq \mu_{Nj} = \max \left\{ 2\widehat{M}_{Nj}, \frac{H_{Nj}}{\rho_{Nj} \eta_{Nj} \zeta_{Nj}} \right\}, \quad j = 0, 1, \dots, n_u, \end{aligned} \quad (38)$$

where  $H_{Nj} = \alpha_{Nj} / \gamma_{Nj}$ ,  $\zeta_{Nj} \in (0, 1)$  and  $W_{Nj}(\Phi_{Nj}) = \rho_{Nj} \eta_{Nj} (1 - \zeta_{Nj}) \Phi_{Nj}^2, j = 0, 1, \dots, n_u$ .

As the dynamics in (21) and (22) are smooth and (37) and (38) hold, it is possible to apply theorem 4.18, p. 172 in Reference 19, which guarantees the boundedness and the ultimate boundedness of the evolution of each  $\Phi_{Nj}$ , and the ultimate bound is  $W_{Na}^{-1}(W_{Nb}(\mu_{Ni})) = \mu_{Ni}, j = 0, 1, \dots, n_w$ .

### 3.2 | Closed-loop dynamics and the Lyapunov-like function candidate

The closed-loop error dynamics are obtained through (1)–(3), (7), and (11) and they are

$$\dot{x}_e = A_m x_e + B_m \hat{\Phi}_R^{-1} \Phi_e w - B_m \hat{\Phi}_R^{-1} S y_e w^T \Gamma_\beta w - B_m \hat{\Phi}_R^{-1} u_N - \mathcal{G}, \quad (39a)$$

$$\dot{\phi}_e = f_\phi(\phi, \phi_e, y_e, w), \quad (39b)$$

with  $f_\phi$  being a smooth vector field for the dynamics of integral part of the adaptive gains  $\phi_e$ . The entries of  $\phi_e$  can be collected in the matrix  $\Phi_e \in \mathbb{R}^{n_u \times n_w}$  obtained by deriving  $\Phi_e$  in (26). After some algebraic manipulations, the dynamics of  $\Phi_e$  are

$$\dot{\Phi}_e = -\Phi_e = -S^T y_e w^T \Gamma_\alpha - F, \quad \text{with } F = -\sigma_\phi(\|\phi\|)\Phi_e \Gamma_\rho. \quad (40)$$

As the control action  $u_N$ , computed either as (19) or (20), is discontinuous, the vector field of system (39a) is discontinuous, thus it is not possible to use the theory presented in Reference 19 to prove the ultimate boundedness of the closed-loop error system in (39). Consequently, the theory presented in Appendix A for Filippov systems is used, and the differential equation (39) is replaced with the corresponding differential inclusion

$$\dot{\tilde{x}}_e \in \mathbf{K}[\mathcal{J}](t, \tilde{x}_e), \quad (41)$$

where  $\tilde{x}_e$  is defined in (26) and  $\mathbf{K}[\mathcal{J}](t, \tilde{x}_e)$  is the Filippov set valued map for the discontinuous closed-loop vector field, which is computed as

$$\begin{aligned} \mathbf{K}[\mathcal{J}](t, \tilde{x}_e) &= \mathbf{K} \left[ \begin{array}{c} A_m x_e + B_m \hat{\Phi}_R^{-1} \Phi_e w - B_m \hat{\Phi}_R^{-1} S y_e w^T \Gamma_\beta w - B_m \hat{\Phi}_R^{-1} u_N - \mathcal{G} \\ f(\phi, \phi_e, y_e, w) \end{array} \right] \\ &= \left[ \begin{array}{c} A_m x_e + B_m \hat{\Phi}_R^{-1} \Phi_e w - B_m \hat{\Phi}_R^{-1} S y_e w^T \Gamma_\beta w - B_m \hat{\Phi}_R^{-1} \mathbf{K}[u_N] - \mathcal{G} \\ f(\phi, \phi_e, y_e, w) \end{array} \right]. \end{aligned} \quad (42)$$

In the case of the EMRAC-UV,  $\mathbf{K}[u_N]$  is

$$\mathbf{K}[u_N] = \mathbf{K}[u_N^{(uv)}] = S^T \Phi_{N0} \mathbf{K} \left[ \frac{y_e}{\|y_e\|} \right], \quad \text{with } \mathbf{K} \left[ \frac{y_e}{\|y_e\|} \right] = \begin{cases} \bar{y}_e, & \text{if } \|y_e\| \neq 0, \\ \mathcal{B}_u, & \text{if } \|y_e\| = 0, \end{cases} \quad (43)$$

with  $\mathbf{K} \left[ \frac{y_e}{\|y_e\|} \right]$  being the set-valued vector function in Reference 36, where  $\bar{y}_e$  is the unit vector in the direction of  $y_e$  and  $\mathcal{B}_u$  is the closed unit sphere in  $\mathbb{R}^{n_u}$  centered in the origin.

For the EMRAC-EW,  $\mathbf{K}[u_N]$  is

$$\mathbf{K}[u_N] = \mathbf{K}[u_N^{(ew)}] = S^T \Phi_N \mathbf{K}[\psi(y_e)], \quad (44)$$

with

$$\mathbf{K}[\psi(y_e)] = \left[ \mathbf{K}[\text{sgn}(y_{e1})] \quad \mathbf{K}[\text{sgn}(y_{e2})] \quad \dots \quad \mathbf{K}[\text{sgn}(y_{e n_u})] \right]^T, \quad (45)$$

where  $\mathbf{K}[\text{sgn}(y_{ej})]$ ,  $j = 1, 2, \dots, n_u$ , is the set-valued map

$$\mathbf{K}[\text{sgn}(y_{ej})] = \begin{cases} -1, & \text{if } y_{ej} < 0, \\ [-1, 1], & \text{if } y_{ej} = 0, \\ 1, & \text{if } y_{ej} > 0. \end{cases} \quad (46)$$

For system (41), the Lyapunov-like function is selected as

$$V(\tilde{x}_e) = \tilde{x}_e^T \tilde{P} \tilde{x}_e, \quad (47)$$

where  $\tilde{P}$  is the strictly positive matrix defined in (27). The Lyapunov-like function (47) can be bounded as

$$W_1(\tilde{x}_e) \leq V(\tilde{x}_e) \leq W_2(\tilde{x}_e), \quad \text{with} \quad W_1(\tilde{x}_e) = \lambda_{\min}(\tilde{P}) \|\tilde{x}_e\|^2, \quad W_2(\tilde{x}_e) = \lambda_{\max}(\tilde{P}) \|\tilde{x}_e\|^2, \quad (48)$$

where  $W_1, W_2 \in \mathcal{K}_\infty$ . Moreover,  $V(\tilde{x}_e)$  can be rewritten as

$$V(\tilde{x}_e) = V(x_e, \phi_e) = x_e^T P_e x_e + \phi_e^T \left( \Gamma_\alpha^{-1} \otimes P_\phi^{-1} \right) \phi_e = x_e^T P_e x_e + \sum_{j=1}^{n_w} \phi_{ej}^T \frac{P_\phi^{-1}}{\alpha_j} \phi_{ej} = x_e^T P_e x_e + \text{tr} \left[ \Phi_e^T P_\phi^{-1} \Phi_e \Gamma_\alpha^{-1} \right]. \quad (49)$$

As the function  $V(\tilde{x}_e)$  is smooth, its generalized derivative can be computed as  $\dot{V} = \nabla V^T \mathbf{K}[\mathfrak{S}]$  (see also Appendix A). By using (3), (12), (40), and (42), after some algebraic manipulations,  $\dot{V}$  takes the following form

$$\begin{aligned} \dot{V} = & -x_e^T Q x_e + 2y_e^T \hat{\Phi}_R^{-1} \Phi_e w - 2y_e^T S P_\phi^{-1} S^T y_e w^T \Gamma_\rho w - 2y_e^T \hat{\Phi}_R^{-1} \mathbf{K}[u_N] \\ & - 2\text{tr} \left[ \Phi_e^T P_\phi^{-1} S^T y_e w^T \right] - 2\text{tr} \left[ \Phi_e^T P_\phi^{-1} F \Gamma_\alpha^{-1} \right] - 2x_e^T P_e \mathcal{G}. \end{aligned} \quad (50)$$

Now, as

$$y_e^T \hat{\Phi}_R^{-1} \Phi_e w = \text{tr} \left[ y_e^T \hat{\Phi}_R^{-1} \Phi_e w \right] = \text{tr} \left[ y_e^T S P_\phi^{-1} \Phi_e w \right] = \text{tr} \left[ w^T \Phi_e^T P_\phi^{-1} S^T y_e \right] = \text{tr} \left[ \Phi_e^T P_\phi^{-1} S^T y_e w^T \right], \quad (51a)$$

$$\text{tr} \left[ \Phi_e^T P_\phi^{-1} F \Gamma_\alpha^{-1} \right] = -\sigma_\phi \text{tr} \left[ \Phi_e^T P_\phi^{-1} \Phi \Gamma_\rho \Gamma_\alpha^{-1} \right] = -\sigma_\phi \sum_{j=1}^{n_w} \phi_{ej}^T \frac{\rho_j}{\alpha_j} P_\phi^{-1} \phi_j = -\sigma_\phi \phi_e^T \left( \Gamma_\rho \Gamma_\alpha^{-1} \otimes P_\phi^{-1} \right) \phi, \quad (51b)$$

$$y_e^T S P_\phi^{-1} S^T y_e w^T \Gamma_\rho w \geq 0, \quad \forall y_e \in R^{n_u}, \quad \text{and} \quad \forall w \in R^{n_w}, \quad (51c)$$

$\dot{V}$  can be upper-bounded as

$$\dot{V} \leq -x_e^T Q x_e - 2y_e^T \hat{\Phi}_R^{-1} \mathbf{K}[u_N] - 2x_e^T P_e \mathcal{G} - 2 \left[ -\sigma_\phi (\|\phi\|) \phi_e^T \left( \Gamma_\rho \Gamma_\alpha^{-1} \otimes P_\phi^{-1} \right) \phi \right]. \quad (52)$$

Furthermore, by using (17), (35), Lemma 1 and  $\Phi_R^{-1} = S P_\phi^{-1}$ , after some algebraic manipulations,  $\dot{V}$  can be further upper-bounded as

$$\begin{aligned} \dot{V} & \leq -\frac{3}{4} \lambda_{\min}(Q) \|x_e\|^2 - \lambda_{\min}(Q) \left\| \frac{x_e}{2} + \frac{2P_e \mathcal{G}}{\lambda_{\min}(Q)} \right\|^2 + \frac{4\|P_e\|^2 \|\mathcal{G}\|^2}{\lambda_{\min}(Q)} \\ & \quad - 2y_e^T S P_\phi^{-1} \mathbf{K}[u_N] - 2 \left[ -\sigma_\phi (\|\phi\|) \phi_e^T \left( \Gamma_\rho \Gamma_\alpha^{-1} \otimes P_\phi^{-1} \right) \phi \right] \\ & \leq -\frac{3}{4} \lambda_{\min}(Q) \|x_e\|^2 + \frac{4\|P_e\|^2 \mathcal{G}_\infty^2}{\lambda_{\min}(Q)} - 2y_e^T S P_\phi^{-1} \mathbf{K}[u_N] - 2 \left[ -\sigma_\phi (\|\phi\|) \phi_e^T \left( \Gamma_\rho \Gamma_\alpha^{-1} \otimes P_\phi^{-1} \right) \phi \right] \\ & \leq -\frac{3}{4} \lambda_{\min}(Q) \|x_e\|^2 + \frac{4\|P_e\|^2 \mathcal{G}_\infty^2}{\lambda_{\min}(Q)} - 2y_e^T S P_\phi^{-1} \mathbf{K}[u_N] + \frac{3}{4} \lambda_{\min}(Q) \left( \left( 2\hat{M}_\phi + \|\hat{\phi}\| \right)^2 - \|\phi_e\|^2 \right) \\ & \leq -\frac{3}{4} \lambda_{\min}(Q) \|\tilde{x}_e\|^2 + \frac{4\|P_e\|^2 \mathcal{G}_\infty^2}{\lambda_{\min}(Q)} + \frac{3}{4} \lambda_{\min}(Q) \left( 2\hat{M}_\phi + \|\hat{\phi}\| \right)^2 - 2y_e^T S P_\phi^{-1} \mathbf{K}[u_N] \\ & = -\mu_1 \|\tilde{x}_e\|^2 + \mu_2 (\mathcal{G}_\infty) - 2y_e^T S P_\phi^{-1} \mathbf{K}[u_N], \end{aligned} \quad (53)$$

where  $\mu_2$  in (28) is computed by using  $\tilde{\mathcal{G}}_\infty^2 = \mathcal{G}_\infty^2$ .

In the case  $\widehat{G}^T B_m \delta \geq 0$ ,  $\forall t \geq t_0$ , with the same steps,  $\dot{V}$  can be upper-bounded as

$$\dot{V} \leq -\mu_1 \|\tilde{x}_e\|^2 + \mu_2(\widehat{G}_\infty) - 2y_e^T \delta - 2y_e^T S P_\phi^{-1} \mathbf{K}[u_N], \quad (54)$$

where  $\mu_2$  in (28) is computed by using  $\widetilde{G}_\infty^2 = \widehat{G}_\infty^2 < G_\infty^2$ .

### 3.3 | Proof of Theorem 1a

In the case of the EMRAC-UV, from (43) the term  $y_e^T S P_\phi^{-1} \mathbf{K}[u_N]$  in (53) and (54) become

$$y_e^T S P_\phi^{-1} S^T \Phi_{N_0} \mathbf{K} \left[ \frac{y_e}{\|y_e\|} \right] = \begin{cases} \|y_e\| \bar{y}_e^T S P_\phi^{-1} S^T \Phi_{N_0} \bar{y}_e, & \text{if } y_e \neq 0, \\ 0, & \text{if } y_e = 0, \forall v \in K \left[ \frac{y_e}{\|y_e\|} \right], \end{cases}$$

and thus

$$y_e^T S P_\phi^{-1} S^T \Phi_{N_0} \mathbf{K} \left[ \frac{y_e}{\|y_e\|} \right] = \|y_e\| \bar{y}_e^T S P_\phi^{-1} S^T \Phi_{N_0} \bar{y}_e \geq 0. \quad (55)$$

Hence, (53) can be further upper-bounded as

$$\dot{V} \leq -\mu_1 \zeta \|\tilde{x}_e\|^2 - \mu_1(1 - \zeta) \|\tilde{x}_e\|^2 + \mu_2(G_\infty) \leq -W_3(\tilde{x}_e), \quad \text{when } \|\tilde{x}_e\| \geq \sqrt{\frac{\mu_2(G_\infty)}{\mu_1(1 - \zeta)}} = \mu(G_\infty), \quad (56)$$

where  $\zeta \in (0, 1)$  and  $W_3(\tilde{x}_e) \in \mathcal{K}$  is the positive function defined as

$$W_3(\tilde{x}_e) = \mu_1 \zeta \|\tilde{x}_e\|^2. \quad (57)$$

Since (48) and (57) hold, Theorem 3 in Appendix A can be applied, thus the closed-loop error dynamics (39)–(41) are ultimate bounded and the ultimate bound is  $W_1^{-1}(W_2(\mu(G_\infty))) = \sqrt{\frac{\lambda_{\max}(\tilde{P})}{\lambda_{\min}(\tilde{P})}} \mu(G_\infty)$  as stated in Theorem 1a when  $\widetilde{G}_\infty^2 = G_\infty^2$ . Moreover, there exist a  $\mathcal{KL}$ -class function  $\Psi : \mathbb{R}^+ \times \mathbb{R}^+ \rightarrow \mathbb{R}^+$ , a time interval  $\mathcal{T}$  and a function  $\gamma_b \in \mathcal{L}_\infty$  such that the error dynamics are bounded as

$$\|\tilde{x}_e(t)\| \leq \gamma_b(t), \quad \text{with } \gamma_b(t) = \begin{cases} \Psi(\|\tilde{x}_e(t_0)\|, t - t_0), & \text{if } t_0 \leq t < t_0 + \mathcal{T}, \\ \sqrt{\frac{\lambda_{\max}(\tilde{P})}{\lambda_{\min}(\tilde{P})}} \mu(G_\infty), & \text{if } t > t_0 + \mathcal{T}. \end{cases} \quad (58)$$

Consider now the case  $\widehat{G}^T B_m \delta > 0 \forall t \geq t_0$ , along with the decomposition of the disturbance  $\mathcal{G}$  in (6). Under these conditions, by using also (21), (25), there exists a time instant  $t_0^* > t_0$  such that  $\Phi_{N_0} > \delta_\infty / \lambda_{\min}(S P_\phi^{-1} S^T)$ , for all  $t > t_0^*$ . Hence, by considering also (55),  $\dot{V}$  in (54) can be upper bounded as

$$\begin{aligned} \dot{V} &\leq -\mu_1 \|\tilde{x}_e\|^2 + \mu_2(\widehat{G}_\infty) - 2y_e^T \delta - 2\|y_e\| \bar{y}_e^T S P_\phi^{-1} S^T \Phi_{N_0} \bar{y}_e \\ &\leq -\mu_1 \|\tilde{x}_e\|^2 + \mu_2(\widehat{G}_\infty) + 2\|y_e\| \delta_\infty - 2\Phi_{N_0} \lambda_{\min}(S P_\phi^{-1} S^T) \|y_e\| \\ &= -\mu_1 \|\tilde{x}_e\|^2 + \mu_2(\widehat{G}_\infty) - 2\lambda_{\min}(S P_\phi^{-1} S^T) \|y_e\| \left[ \Phi_{N_0} - \frac{\delta_\infty}{\lambda_{\min}(S P_\phi^{-1} S^T)} \right] \\ &\leq -\mu_1 \zeta \|\tilde{x}_e\|^2 - \mu_1(1 - \zeta) \|\tilde{x}_e\|^2 + \mu_2(\widehat{G}_\infty) \leq -W_3(\tilde{x}_e), \quad \text{when } \|\tilde{x}_e\| \geq \sqrt{\frac{\mu_2(\widehat{G}_\infty)}{\mu_1(1 - \zeta)}} = \mu(\widehat{G}_\infty), \end{aligned} \quad (59)$$

where  $\zeta \in (0, 1)$  and  $W_3(\tilde{x}_e) \in \mathcal{K}$  is the function defined in (57). As (48) and (59) hold, similar to the previous case, Theorem 3 in Appendix A can be applied, thus the closed-loop error dynamics (39)–(41) are ultimate bounded, and the ultimate bound is  $W_1^{-1}(W_2(\mu(\hat{\mathcal{G}}_\infty))) = \sqrt{\frac{\lambda_{\max}(\tilde{P})}{\lambda_{\min}(\tilde{P})}} \mu(\hat{\mathcal{G}}_\infty)$  as stated in Theorem 1a when  $\tilde{\mathcal{G}}_\infty = \hat{\mathcal{G}}_\infty$ . Moreover, there exists a  $\mathcal{KL}$ -class function  $\Psi^* : \mathbb{R}^+ \times \mathbb{R}^+ \rightarrow \mathbb{R}^+$ , a time interval  $\mathcal{T}^*$  and a function  $\gamma_b^* \in \mathcal{L}_\infty$  such that the error dynamics are bounded as

$$\|\tilde{x}_e(t)\| \leq \gamma_b^*(t), \quad \text{with} \quad \gamma_b^*(t) = \begin{cases} \gamma_b(t), & \text{if } t_0 \leq t < t_0^*, \\ \Psi^*(\|\tilde{x}_e(t_0^*)\|, t - t_0^*), & \text{if } t_0^* \leq t < t_0^* + \mathcal{T}^*, \\ \sqrt{\frac{\lambda_{\max}(\tilde{P})}{\lambda_{\min}(\tilde{P})}} \mu(\mathcal{G}_\infty), & \text{if } t > t_0^* + \mathcal{T}^*. \end{cases} \quad (60)$$

The boundedness of  $\|\tilde{x}_e\|$ , guaranteed either by (58) or (60), implies the boundedness of  $x_e$ ,  $\phi_e$  and  $\Phi_e$ . As  $x_e$  is bounded (i.e.,  $x_e \in \mathcal{L}_\infty$ ) then  $y_e$  is bounded, and because  $x_m$  is bounded by assumption, then also  $x$  is bounded, while the boundedness of  $x_I$  can be proven as in Reference 34. The boundedness of  $\Phi_e$ ,  $x_e$ ,  $d$ ,  $r$  imply that  $K_X$ ,  $K_R$ ,  $K_I$  and  $K_D$  are bounded. The boundedness of the signals  $x$ ,  $x_e$ ,  $d$ ,  $r$ ,  $\Phi_{N0}$ ,  $K_X$ ,  $K_R$ ,  $K_I$ , and  $K_D$  implies that also  $u$  and  $\dot{x}$  are bounded. Hence, the boundedness of all closed-loop signals remains proven when the EMRAC-UV is used, thus concluding the proof of Theorem 1a.

### 3.4 | Proof of Theorem 1b

In the case  $\hat{\mathcal{G}} = 0$ , by using (34), (43), and (55),  $\dot{V}$  in (52) can be upper-bounded as

$$\begin{aligned} \dot{V} &\leq -x_e^T Q x_e - 2y_e^T \delta - 2\|y_e\| \bar{y}_e^T S P_\phi^{-1} S^T \Phi_{N0} \bar{y}_e \\ &\leq -\lambda_{\min}(Q) \|x_e\|^2 - 2\lambda_{\min}(S P_\phi^{-1} S^T) \|y_e\| \left[ \Phi_{N0} - \frac{\delta_\infty}{\lambda_{\min}(S P_\phi^{-1} S^T)} \right]. \end{aligned} \quad (61)$$

From (21) and (25), there exists a time instant  $t_0^* > t_0$  such that for  $t > t_0^*$ , (61) can be further upper-bounded as

$$\dot{V} \leq -W(x_e), \quad \text{with} \quad W(x_e) = \lambda_{\min}(Q) \|x_e\|^2. \quad (62)$$

According to Appendix A,  $\frac{dV}{dt}(\tilde{x}_e(t), t) \in^{a.e.} \dot{V}(\tilde{x}_e(t), t)$ , thus

$$\frac{dV}{dt}(\tilde{x}_e(t), t) \leq -W(x_e), \quad \text{almost everywhere.} \quad (63)$$

Now, according to References 10,37, from (63) for any closed-loop  $x_e$ -trajectory we have

$$\int_{t_0^*}^{+\infty} W(x_e(\tau)) d\tau \leq V(\tilde{x}_e(t_0^*)). \quad (64)$$

Since  $W(x_e)$  is a continuously differentiable positive-definite function, Barbalat's Lemma can be applied, and  $W(x_e(t))$  converges to zero when  $t \rightarrow +\infty$ .<sup>10,37</sup> Consequently, the state tracking error  $x_e(t)$  converges to zero when  $t \rightarrow +\infty$ , thus concluding the proof of Theorem 1b.

### 3.5 | Proof of Theorem 2

In the case of the EMRAC-EW, when the matrix  $S P_\phi^{-1} S^T$  is diagonal, the term  $y_e^T S P_\phi^{-1} \mathbf{K} [u_N]$  in (53) and (54) becomes

$$y_e^T S P_\phi^{-1} S^T \Phi_N \mathbf{K} [\psi(y_e)] = \sum_{j=1}^{n_u} \tilde{c}_j \Phi_{Nj} y_{ej} \mathbf{K} [\text{sgn}(y_{ej})].$$

When  $y_{ej} = 0$  then  $y_{ej} \mathbf{K} [\text{sgn}(y_{ej})] = 0, \forall v \in \mathbf{K}[0]$ , thus

$$y_e^T S P_\phi^{-1} S^T \Phi_N \mathbf{K} [\psi(y_e)] = \sum_{j=1}^{n_u} \tilde{c}_j \Phi_{Nj} |y_{ej}| \geq 0, \quad \forall y_{ej}, j = 1, \dots, n_u. \quad (65)$$

Hence, (53) can be upper-bounded as in (56). Consequently, as shown in Section 3.3, the closed-loop error dynamics

(39)–(41) are ultimate bounded, and the ultimate bound is  $W_1^{-1}(W_2(\mu(\hat{\mathcal{G}}_\infty))) = \sqrt{\frac{\lambda_{\max}(\tilde{P})}{\lambda_{\min}(\tilde{P})}} \mu(\hat{\mathcal{G}}_\infty)$ .

Moreover, from (22) and (25) there exists a time instant  $t_0^* > t_0$  such that  $\Phi_{Nj} > \delta_{j\infty} / \tilde{c}_j, j = 1, \dots, n_u$  for all  $t > t_0^*$ . Hence, in the case  $\hat{\mathcal{G}}^T B_m \delta > 0, \forall t \geq t_0$ , and the decomposition (6) of the disturbance  $\mathcal{G}$  is used, by using (65) when  $t > t_0^*$ ,  $\dot{V}$  in (54) can be upper bounded as

$$\begin{aligned} \dot{V} &\leq -\mu_1 \|\tilde{x}_e\|^2 + \mu_2(\hat{\mathcal{G}}_\infty) - 2 \sum_{j=1}^{n_u} (\tilde{c}_j \Phi_{Nj} |y_{ej}| - \delta_{j\infty} |y_{ej}|) \\ &\leq -\mu_1 \|\tilde{x}_e\|^2 + \mu_2(\hat{\mathcal{G}}_\infty) - 2 \sum_{j=1}^{n_u} \tilde{c}_j |y_{ej}| \left( \Phi_{Nj} - \frac{\delta_{j\infty}}{\tilde{c}_j} \right) \\ &\leq -\mu_1 \zeta \|\tilde{x}_e\|^2 - \mu_1(1 - \zeta) \|\tilde{x}_e\|^2 + \mu_2(\hat{\mathcal{G}}_\infty) \leq -W_3(\tilde{x}_e), \quad \text{when} \quad \|\tilde{x}_e\| \geq \sqrt{\frac{\mu_2(\hat{\mathcal{G}}_\infty)}{\mu_1(1 - \zeta)}} = \mu(\hat{\mathcal{G}}_\infty), \end{aligned} \quad (66)$$

where  $\zeta \in (0, 1)$  and  $W_3(\tilde{x}_e) \in \mathcal{K}$  is the function defined in (57). As (66) provides the same upper-bound for  $\dot{V}$  given by (59), the proof of the ultimate-boundedness of the closed-loop error dynamics (39)–(41) with ultimate bound given by

$W_1^{-1}(W_2(\mu(\hat{\mathcal{G}}_\infty))) = \sqrt{\frac{\lambda_{\max}(\tilde{P})}{\lambda_{\min}(\tilde{P})}} \mu(\hat{\mathcal{G}}_\infty)$  as well as the boundedness of all closed-loop signals follow equivalently as shown in the proof of Theorem 1a.

Finally, when  $\hat{G} = 0$ , by using (34), (44), and (65),  $\dot{V}$  in (52) can be upper-bounded as

$$\dot{V} \leq -x_e^T Q x_e - 2y_e^T \delta - 2 \sum_{j=1}^{n_u} \tilde{c}_j \Phi_{Nj} |y_{ej}| \leq -x_e^T Q x_e - 2 \sum_{j=1}^{n_u} \tilde{c}_j |y_{ej}| \left( \Phi_{Nj} - \frac{\delta_{j\infty}}{\tilde{c}_j} \right). \quad (67)$$

From (22) and (25), there exists a time instant  $t_0^*$  such that  $\dot{V}$  can be further upper-bounded as in (62) for all  $t > t^*$ . Hence, the convergence to zero of  $x_e$  follow equivalently as shown in the proof of Theorem 1b in Section 3.4, thus also Theorem 2 remains proven.

### 3.6 | Proof of Corollary 1

The proof of Corollary 1 is an extension of the proof of Corollaries 1 and 2 presented in Reference 34 to multi-input systems and an extension of the result presented in Reference 32 to the case the model of the plant is not in control canonical form.

In the case the matrices of the plant (1) are constants then also the matrix  $\hat{\Phi}$  is constant, and thus  $\dot{\Phi}_e = -\dot{\Phi}$  in (40). On the other hand, for time varying matrices,

$$\Phi_e = \hat{\Phi} - S^T y_e w^T \Gamma_\alpha - F.$$

Nevertheless, the approximation (32) yields

$$\dot{\Phi}_e \approx -S^T y_e w^T \Gamma_\alpha - F = -\dot{\Phi}.$$

Consequently, (40) still holds, and therefore the proofs of Theorems 1 and 2 follow identically.

## 4 | APPLICATION OF MULTI-INPUT EMRAC SOLUTIONS TO SPACE ROBOTIC ARMS

The free-flying space robot system is the spacecraft platform whose attitude is controlled during the manipulation.<sup>24,38</sup> When the position and orientation of the base-spacecraft are kept fixed by the AOCS<sup>39</sup> during the postcapturing phase of a noncooperative micro-satellite target, the model of a free-flying robotic manipulator with  $n$  links is expressed as

$$B(q)\ddot{q} + C(q, \dot{q})\dot{q} + F_v\dot{q} + J_p^T(q)f_p = \tau, \quad (68)$$

where  $q \in \mathbb{R}^n$  is the vector of the joint variables,  $\tau \in \mathbb{R}^n$  is the vector of the torques and forces provided to each joint (control variables),  $B(q) \in \mathbb{R}^{n \times n}$  is the inertial matrix,  $C(q, \dot{q}) \in \mathbb{R}^{n \times n}$  is a matrix such that  $C(q, \dot{q})\dot{q}$  is the vector of Coriolis and centrifugal torques and forces,  $F_v \in \mathbb{R}^{n \times n}$  is the matrix of the damping coefficients,  $J_p(q) \in \mathbb{R}^{3 \times n}$  is the submatrix of the geometric Jacobian of the manipulator relating the joint velocities to the end-effector linear velocity. The force  $f_p \in \mathbb{R}^3$  is the reaction disturbance force provided by the AOCS of the noncooperative target, and is modeled in accordance with an ideal cold gas thruster on the target spacecraft. Specifically, the AOCS measures the first- or second-order derivatives of the attitude or orbit drifts, and feedbacks them for attitude or orbit control.<sup>40</sup> For this study it is assumed that the target spacecraft uses the cold gas thruster as AOCS actuator, as it is a common solution for micro and small spacecrafts.<sup>41</sup> Furthermore, it is assumed that (i) the thruster control constant  $\kappa$ , which depends on the fuel used and the mechanical design of the nozzle of the thruster,<sup>42</sup> is a positive constant; (ii) the target is rigidly moved with the end-effector of the service robotic arm during the postcapturing phase, thus the acceleration drift of the target measured by the AOCS sensor is that of the end-effector (i.e.,  $\ddot{p}$ ); (iii) the reaction forces are sensitive to the second-order derivative of the longitudinal orbital change as this variation is usually used by AOCS to compensate for external forces causing target orbital changes; and (iv) the residual orbital station-keeping and hypothetical anti-capture controls are activated during the entire postcapture servicing phase and provide uncooperative forces proportional to the second derivatives of orbital changes through the thruster control constant  $\kappa$  to resist the manipulation action. Hence, the following simplified model is used to account for the effect of the AOCS onto the manipulator dynamics

$$f_p = \kappa\ddot{p}. \quad (69)$$

According to Reference 43, when a full-state FL is used for compensating the term  $C(q, \dot{q})\dot{q}$  in (68) to make the closed-loop system behave as an  $n$ -dimensional decoupled mass-spring-damper system with stiffness  $K \in \mathbb{R}^{n \times n}$  and damping matrix  $\Theta \in \mathbb{R}^{n \times n}$ , the resulting plant to control takes the form in (1) with  $\hat{G} = 0$ ,  $d = 0$ ,  $E = 0$ ,  $n_u = n$ ,  $n_x = 2n$  and

$$x = \begin{bmatrix} q \\ \dot{q} \end{bmatrix}, \quad A = \begin{bmatrix} \mathcal{O}_{n,n} & I_n \\ -K & -(\Theta + F_v) \end{bmatrix}, \quad B = \begin{bmatrix} \mathcal{O}_{n,n} \\ I_n \end{bmatrix}, \quad \mathcal{G} = B\delta, \quad (70a)$$

$$\delta = \delta_1 + \delta_2, \quad \delta_1 = (I_n - B^{-1}\hat{B})y + B^{-1}(\hat{C}(q, \dot{q}) - C(q, \dot{q}))\dot{q}, \quad y = -Kq - \Theta\dot{q}, \quad \text{and} \quad \delta_2 = B^{-1}J_p^T f_p. \quad (70b)$$

where  $\hat{B}(q)$  and  $\hat{C}(q, \dot{q})$  are estimates of the matrices  $C(q, \dot{q})$  and  $B(q)$ , respectively. Similarly to the robust control design in Reference 43, as the joint positions are confined in a finite set, and saturations exist on the maximum velocities and accelerations of the motors, then the resulting nonmeasurable disturbance  $\delta$  is bounded. Notice that for system (70a) the interaction force  $f_p$  and friction have not been compensated. Moreover, the matrices  $K$  and  $\Theta$  are diagonal.

For the robotic manipulator, EMRAC solutions can be designed for imposing reference trajectories in the joint space, despite the imperfect compensation of the robot nonlinearities, parameter uncertainties and disturbances.

The reference model for imposing a reference trajectory denoted as  $q_R(t)$  takes the form in (2), where  $E_m = 0$  and

$$x_m = \begin{bmatrix} q_m \\ \dot{q}_m \end{bmatrix}, \quad A_m = \begin{bmatrix} \mathcal{O}_{n,n} & I_n \\ -K & -\Theta \end{bmatrix}, \quad B_m = \begin{bmatrix} \mathcal{O}_{n,n} \\ I_n \end{bmatrix}, \quad x_m(0) = \begin{bmatrix} q_R(0) \\ \dot{q}_R(0) \end{bmatrix}, \quad r(t) = \ddot{q}_R(t) + Kq_R(t) + \Theta\dot{q}_R(t). \quad (71)$$

Hence, the matching conditions (3) are satisfied and  $S = I_n$ .

In what follows, the EMRAC solutions that are used for correcting the imperfect FL strategy and imposing trajectories in the joint space are referred to as EMRAC-FL strategies. Moreover, to further test the robustness of the novel EMRAC



algorithms, EMRAC solutions with no feedback linearization (NFL) control action are also tested when the reference model is set as in (71). These EMRAC solutions are named as EMRAC-NFL strategies.

Consequently, four EMRAC solutions denoted as EMRAC-UV-FL, EMRAC-EW-FL, EMRAC-UV-NFL, and EMRAC-EW-NFL are tested and compared for a case study.

## 5 | NUMERICAL RESULTS

The multi-input EMRAC solutions are tested for a three-link anthropomorphic arm whose fundamental parameters are reported in Table 1.

The simulation scenario is set to emulate the working conditions of a noncooperative interaction between a micro-satellite and the robotic arm in the post-capturing phase (see also Section 4). For this case study, the micro-satellite body is modeled as an unknown load at the end-effector, with cubic shape of side 1 m and mass  $m_{\text{load}} = 100$  kg (see also Figure 1 for a schematic of the manipulator within the simulation environment, notice that the servicing spacecraft model in Figure 1 is based on SpaceX dragon for illustration purposes). The satellite thrusters try to counteract the trajectory imposed by the space robotic arm, thus generating the disturbance  $f_p$  in (69) (or equivalently the disturbance  $\delta_2$  in (70b)). Furthermore, as the mass of the micro-satellite is supposed to be unknown, the resulting FL control action provides an imperfect compensation (i.e.,  $\hat{B} \neq B$  and  $\hat{C} \neq C$ ), thus generating the disturbance term  $\delta_1$  in (70b).

The path to be imposed to the end-effector position in the operational space is shown Figure 2A. The position on the path (i.e., the trajectory) is obtained by using two fifth-order interpolating polynomials. The resulting reference trajectory, denoted as  $p_R(t)$ , lasts 250 s, and consists of five submaneuvers, which are listed in Table 2.

The trajectory in the operational space is converted into the trajectory in the joint space by using the second-order closed-loop inverse kinematic algorithm presented in Reference 43. The resulting reference joint positions and speeds are depicted in Figure 2B and C, respectively.

TABLE 1 Parameters of the three-degree-of-freedom manipulator.

Link	Length (m)	Mass (kg)	Diameter (m)
1	$L_1 = 0.5$	$m_{\ell_1} = 50$	$D_1 = 0.4$
2	$L_2 = 4$	$m_{\ell_2} = 200$	$D_2 = 0.4$
3	$L_3 = 4$	$m_{\ell_3} = 200$	$D_3 = 0.4$

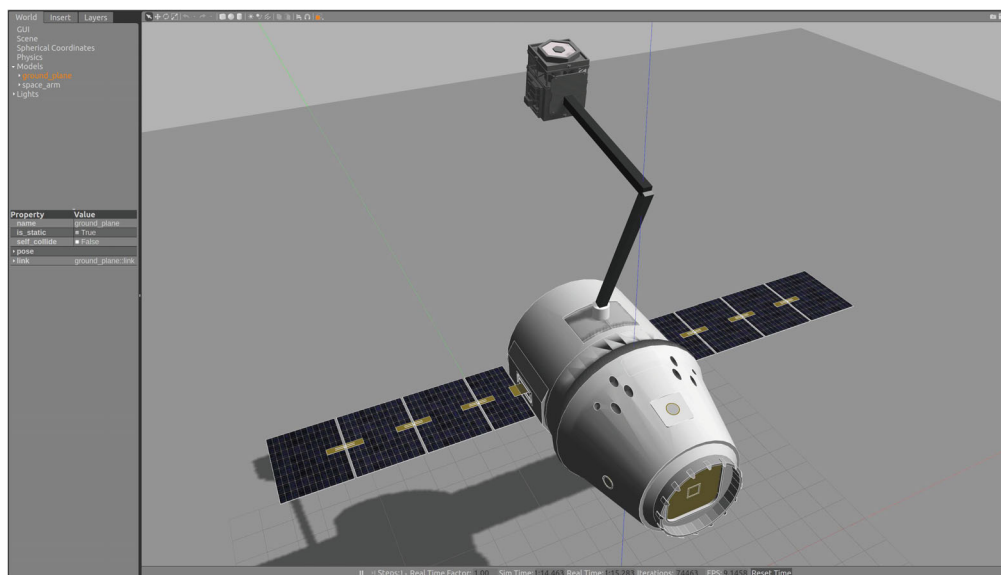


FIGURE 1 The three-link-anthropomorphic arm within the Gazebo-robot operating system simulation environment.

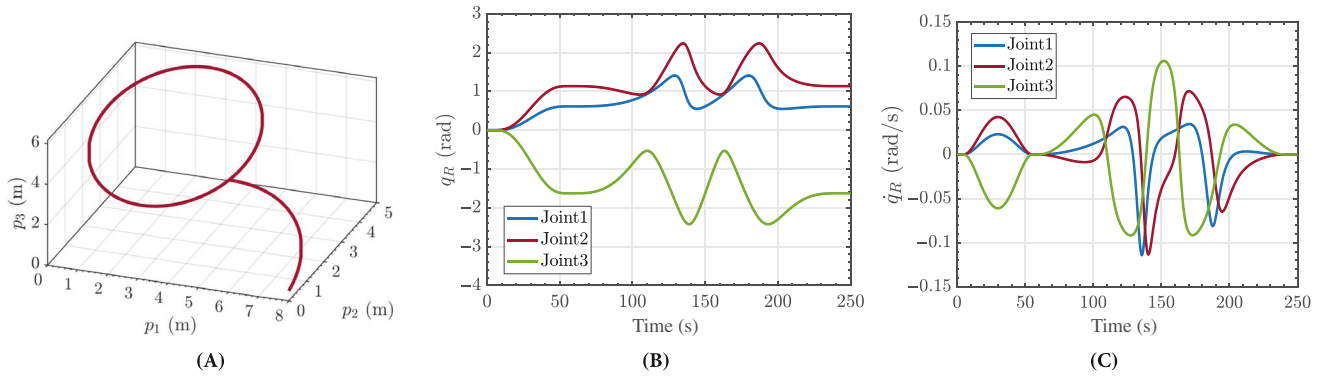


FIGURE 2 Reference trajectory: (A) path in the operational space, (B) reference joint position, and (C) reference joint speed.

TABLE 2 Trajectory of the end effector.

Identifier	Time interval (s)	Description
INIT	$[t_0, t_1]$ , with $t_0 = 0$ and $t_1 = 55$	Initial trajectory with $p_R(t_0) = [8 \ 0 \ 0.5]^T$ m, $p_R(t_1) = \bar{p} = [5 \ 3 \ 4]^T$ m, and $\dot{p}_R(t_0) = \dot{p}_R(t_1) = 0$
First-STST	$[t_1, t_2]$ , with $t_2 = 60$	First steady-state at $\bar{p}$
First-LAP	$[t_2, t_3]$ , with $t_3 = 150$	First lap on the circumference with radius 2.5 m centered in $p_C = [2.5 \ 3 \ 4]^T$ m
Second-LAP	$[t_3, t_4]$ , with $t_4 = 240$	Second lap on the circumference
Second-STST	$[t_4, t_5]$ , with $t_5 = 250$	Second steady-state at $\bar{p}$

The matrices of the reference model (2) have been chosen as in (71) with  $K = 10^{-3} \text{diag}(6.7, 2, 1)$  and  $\Theta = 10^{-2} \text{diag}(16.8, 9, 6.2)$ , while the adaptive weights have been selected as a trade-off between convergence time and reactivity of the control actions. Furthermore, similarly to References 12,33, in order to avoid unwanted chattering phenomena, the discontinuous terms in (19) and (20) have been smoothed as

$$\frac{y_e}{\|y_e\|} = \frac{y_e}{\|y_e\| + \epsilon_0}, \quad \text{and} \quad \text{sgn}(y_{ej}) = \frac{y_{ej}}{|y_{ej}| + \epsilon_j}, \quad j = 1, 2, 3, \quad (72)$$

where  $\epsilon_j, j = 0, 1, 2, 3$ , are strictly positive constants.

To challenge the ability of the closed-loop system to adjust to unknown working conditions, the adaptive gains of the four EMRAC solutions have been initialized to zero. Hence, no preliminary knowledge of the plant is used to initialise the EMRAC adaptive mechanisms.

In addition to the four EMRAC solutions, four benchmark controllers have been designed and implemented. The benchmark controllers are (i) a PID controller embedded in ROS (denoted as ROS-PID) and (ii) three full-state FL-based strategies, augmented with a proportional-integral controller (PI-FL), a proportional derivative controller (PD-FL), or the robust strategy in Reference 44 (ROBUST-FL).

The feedback gains of the PI-FL strategy have been selected through a trial-and-error approach, with the aim to preserve closed-loop stability and minimize the tracking error. The proportional ( $K_P$ ) and derivative ( $K_D$ ) gains of the PD-FL control action have been chosen to have ideal linear closed-loop dynamics given by the eigenvalues of the matrix  $A_m$  in (71), thus they have been set as  $K_P = K$  and  $K_D = \Theta$ , respectively. For the same reason, for the ROBUST-FL controller, the proportional feedback gain  $K_{rb}$  weighting the state tracking error has been selected as  $K_{rb} = [K \ \Theta]$ , while a heuristic approach has been used to tune (i) the gain that modulates the magnitude of the robust sliding mode-based control action (indicated as  $\rho_{rb}$ ) and (ii) the threshold modulating the boundary layer within which the tracking error is allowed to vary (indicated as  $\epsilon_{rb}$ ). Specifically,  $\rho_{rb}$  and  $\epsilon_{rb}$  have been heuristically selected respectively as the largest value and the smallest value which allow to avoid chattering in the control action.

For the implementation in the ROS environment detailed in Appendix B, the EMRAC control solutions and the benchmark controllers have been discretized with a sampling time  $T_s = 5$  ms, with the reference model and the required

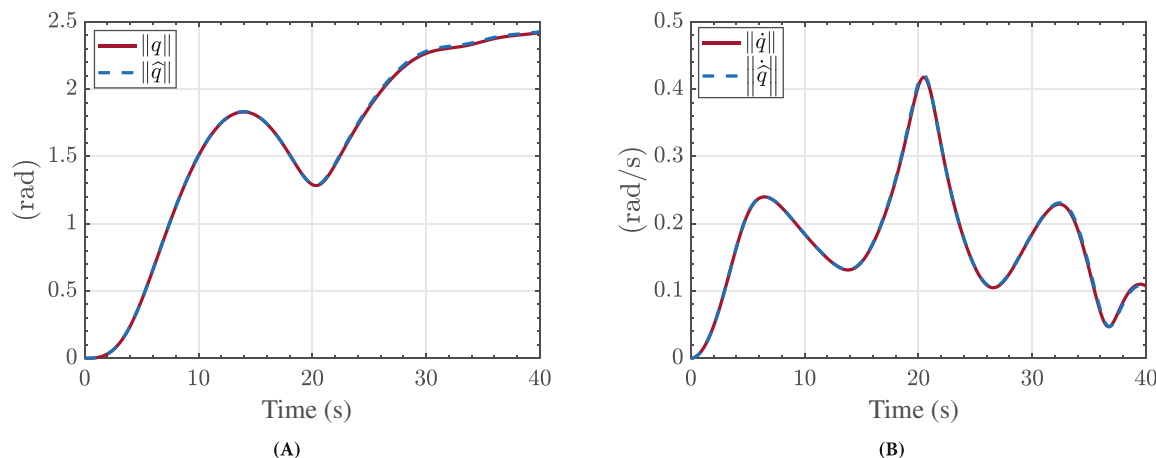


**FIGURE 3** Validation of the mathematical model used for the design of the feedback linearization control action, where  $\hat{q}$  and  $\dot{\hat{q}}$  are the solution of the model, while  $q$  and  $\dot{q}$  are provided by the detailed simulator under nominal conditions (i.e.,  $m_{\text{load}} = 0$  and  $f_p = 0$ ): (A) position and (B) speed.

integrators being discretized by using the Tustin method. Furthermore, the benchmark controllers and the EMRAC solutions run in the ROS environment with a real-time factor equal to 1 during the simulations.

For implementing the control strategies requiring the nominal full-state FL control action, that is, EMRAC-UV-FL, EMRAC-EW-FL, PI-FL, PD-FL, and ROBUST-FL, a mathematical model of the robotic arm has been developed by assuming  $m_{\text{load}} = 0$  and  $f_p = 0$  (nominal robotic arm model). The effectiveness of the designed mathematical model to reproduce the dynamics of the simulator in Appendix B under nominal conditions is shown in Figure 3, where the response of the simulator and the solution of the mathematical model of the robot are depicted when the torques at the joints are  $\tau_i = M_i \sin(2\pi/20t)$ , with  $i = 1, 2, 3$ , and  $M_1 = 100$  Nm,  $M_2 = 70$  Nm and  $M_3 = 40$  Nm. However, the presence of the mass of the micro-satellite and the disturbance force (69) severely alter the plant dynamics, thus requiring closed-loop control systems for tracking the reference trajectory.

## 5.1 | Closed-loop dynamics

The norm of the closed-loop tracking error in the joint space provided by the four EMRAC solutions is depicted in Figure 4. The norm of the joint speed error never exceeds 0.01 rad/s as shown in Figure 4B. Furthermore, Figure 4A shows that the norm of the joint position error is always below 0.04 rad, except for the EMRAC-UV-NFL, which, however, remains below 0.075 rad.

When  $t > t^* = 35$  s, Figure 4A also shows that the norm of the residual joint position error is much smaller than the magnitude of each reference joint position in Figure 2B. Hence, better tracking of the reference trajectory in the operational space is expected when the time exceeds the threshold  $t^*$ . This is confirmed by Figure 5A, which shows that when  $t > t^*$  the norm of the position tracking error remains below 10 cm. The highest values of the position tracking errors are at the beginning of the maneuvers (i.e., within the INIT sub-maneuvers) due to the zero initialization of the adaptive gains of the EMRAC solutions. Indeed, during the initial part of the maneuvers, the control gains are not tuned for precisely compensating the unmodeled dynamics and the disturbance  $f_p$ . Furthermore, the effect of the zero initialization conditions on the tracking error is more severe for the EMRAC-NFL solutions, where also the initial contribution of the nominal FL action is excluded. However, as time evolves, the control gains adapt to the actual operating condition, resulting in better tracking of the reference trajectory in the operational space. Specifically, when the initialisation maneuver is completed (i.e.,  $t > 55$  s), the residual position error in the operational space remains below 3.5 cm for the EMRAC-NFL solutions, while for the EMRAC-FL strategies the 3.5 cm threshold is exceeded only for a time interval of about 10 s at the end of the first-LAP maneuver (see also Figure 5A). Furthermore, the residual speed error is below 0.020 m/s for all the adaptive solutions, as shown in Figure 5B. As the tracking errors provided by the EMRAC solutions for  $t > t^*$  are negligible when compared to the magnitude of the reference trajectory, a precise tracking of the reference path is obtained as shown in Figure 6.

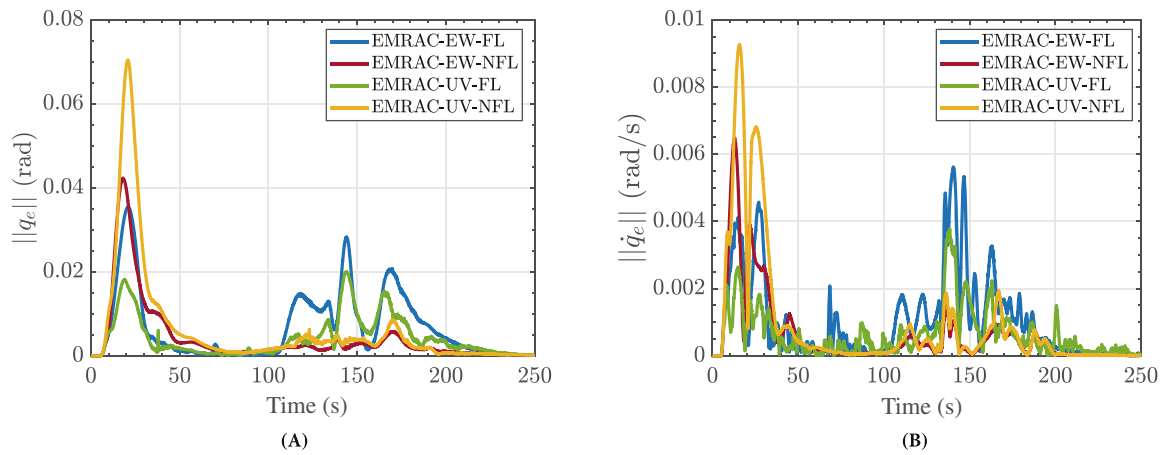


**FIGURE 4** Enhanced model reference adaptive control tracking performance in the joint space: (A) norm of the joint position tracking error and (B) norm of the joint speed tracking error.

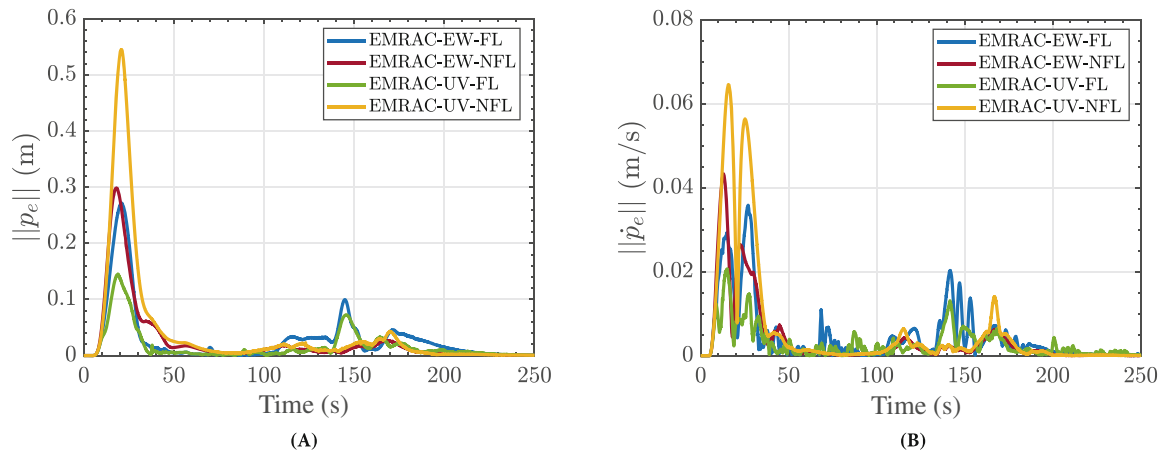


**FIGURE 5** Enhanced model reference adaptive control tracking performance in the operational space: (A) norm of the position tracking error and (B) norm of the speed tracking error.

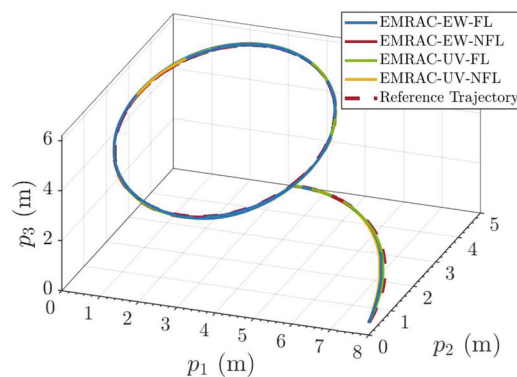


**FIGURE 6** Closed-loop trajectories with the implemented enhanced model reference adaptive controllers.

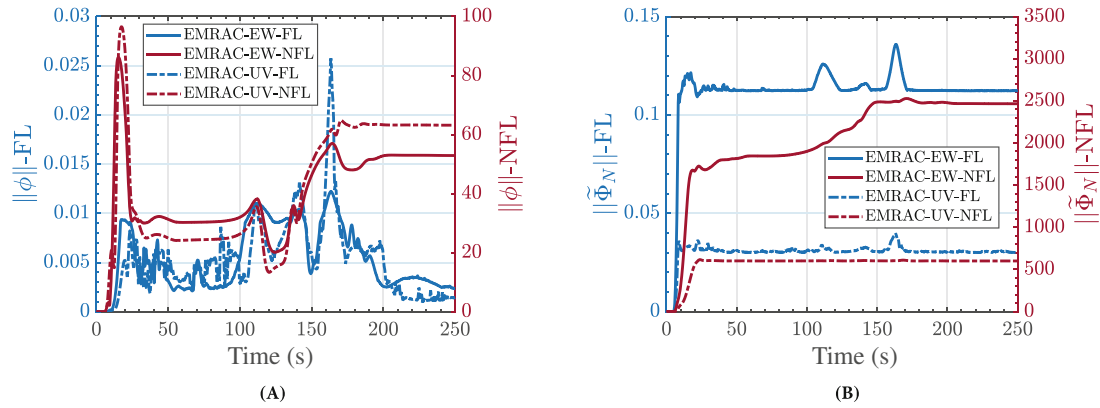


**FIGURE 7** Norm of the integral part of the EMRAC adaptive gains for: (A) the continuous control actions (i.e.,  $\|\phi\|$ ) and (B) the discontinuous control action, where  $\tilde{\Phi}_N = \Phi_N$  for the EMRAC-EW solutions and  $\tilde{\Phi}_N = \Phi_{N0}$  for the EMRAC-UV strategies, respectively.

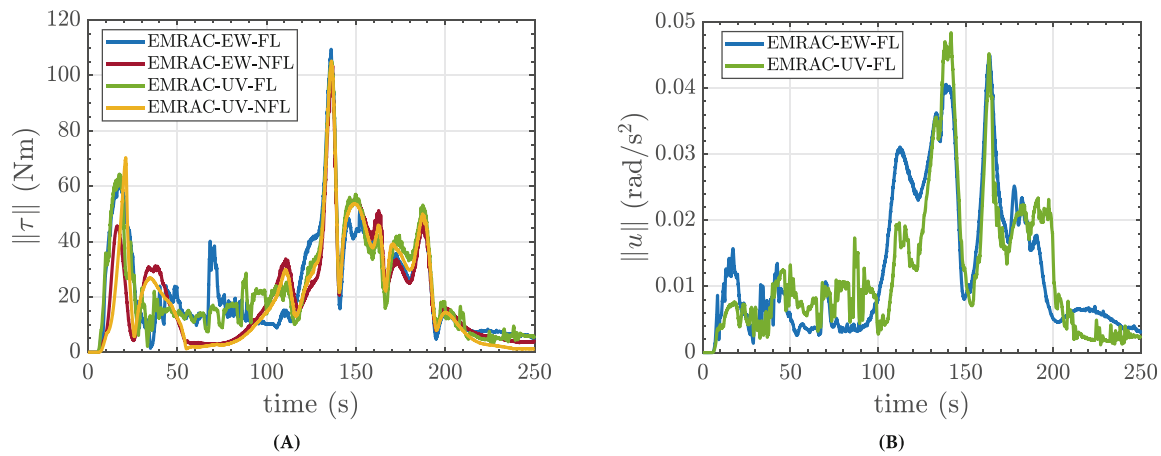


**FIGURE 8** (A) Norm of the demanded torques by the enhanced model reference adaptive control (EMRAC) solutions and (B) norm of the demanded accelerations by the EMRAC-FL solutions.

Figure 7A,B shows the bounded evolution of the norm of the integral part of the adaptive gains for the continuous control action and discontinuous control action, respectively, while the proportional part of the adaptive gains is bounded as the residual tracking error in Figure 4 is bounded. Consequently, Figure 7 confirms the ability of the  $\sigma$ -modification strategies embedded within the EMRAC adaptive laws to prevent an unbounded drift of the adaptive control gains also in presence of persistent disturbances that could ultimately jeopardize the tracking of the reference trajectory.<sup>45</sup> Without the  $\sigma$ -modification strategy in (24), the adaptive gains of the discontinuous control actions diverge, thus resulting in chattering in the control action, which could damage the robot actuators or induce closed-loop instability.

As the control gains and the state variables are bounded, the torque demanded at each joint is bounded, as depicted in Figure 8A, where the norm of the torque is shown for each EMRAC solution. The demanded torques coincide with the control action for the EMRAC-NFL solutions. For the EMRAC-FL solutions, the control action is the required acceleration to each joint, which is also bounded, see Figure 8B. As the unit of measurement of the control action for the EMRAC-FL solutions is different from that of the EMRAC-NFL solutions, the order of magnitude of the corresponding adaptive control gains varies significantly, as depicted in Figure 7.

## 5.2 | Evaluation of the closed-loop performance via KPIs

To quantitatively compare the EMRAC solutions to the benchmark controllers, the root mean square error (RMSE) and the maximum error (ME) are used as KPIs for measuring the closed-loop tracking performance. By denoting as  $\ell$  a

closed-loop vector signal of interest, the corresponding RMSE and the ME are computed as

$$\text{RMSE}_{\|\ell\|} = \sqrt{\frac{1}{t_f - t_i} \int_{t_i}^{t_f} \|\ell_R(t) - \ell(t)\|^2 dt} \quad \text{and} \quad \text{ME}_{\|\ell\|} = \max_{t \in [t_i, t_f]} \{\|\ell_R(t) - \ell(t)\|\}, \quad (73)$$

where  $\ell_R$  is the reference value for the signal  $\ell$ , while  $t_i$  and  $t_f$  are the initial and final time instants, respectively, delimiting the time interval on which the KPIs are computed.

The control effort is measured by the integral of the norm of the demanded torque normalized with time ( $I_{\|\tau\|}$ ), and the maximum norm of the torque ( $M_{\|\tau\|}$ ) defined as

$$I_{\|\tau\|} = \frac{1}{t_f - t_i} \int_{t_i}^{t_f} \|\tau(t)\| dt \quad \text{and} \quad M_{\|\tau\|} = \max_{t \in [t_i, t_f]} \{\|\tau(t)\|\}. \quad (74)$$

The KPIs in (73) and (74) are computed for each submaneuver in Table 2. Table 3 shows the tracking performance KPIs for the joint position and speed, and the KPIs for the control effort, while Table 4 shows the tracking performance KPIs for the position and speed of the end-effector. As the PD with FL and the ROS-PID become unstable while performing the second lap of the circumference, it was not possible to compute the KPIs for the second-LAP and second-STST submaneuvers.

The following remarks are based on Table 3 and Table 4.

- All EMRAC solutions outperform the PD controller for the sub-manuevers where the KPIs for the PD algorithm can be computed (i.e., over the time intervals before the closed-loop stability is lost). For instance, compared to the PD controller, the EMRAC solutions reduce the  $\text{RMSE}_{\|q\|}$  and  $\text{RMSE}_{\|p\|}$  by at least four times and 2.5 times during the INIT-maneuver, respectively. The reduction of the KPIs becomes even more significant over the first-STST and first-LAP submaneuvers. Specifically, for these submaneuvers, the adaptive solutions reduce, for instance, the  $\text{RMSE}_{\|q\|}$  and  $\text{RMSE}_{\|p\|}$  by at least 70 and 23 times, respectively (see the results for EMRAC-UV-NFL and EMRAC-EW-FL, computed over the first-STST maneuver) which result in a reduction of at least 24 and 29 times of the  $\text{RMSE}_{\|p\|}$  and  $\text{RMSE}_{\|q\|}$ , respectively.
- All EMRAC solutions provide better tracking performance compared to the built-in ROS-PID controller over all sub-manuevers before the ROS-PID solution becomes unstable. For instance, over the INIT maneuver, the adaptive solutions reduce the  $\text{RMSE}_{\|p\|}$  by a factor that ranges from 2.5 times and up to nine times. Furthermore, in the first-STST maneuver, the adaptive solutions provide a reduction of the  $\text{ME}_{\|q\|}$  and  $\text{ME}_{\|p\|}$  in excess of 14 and 50 times, respectively, which corresponds to a reduction of the  $\text{ME}_{\|p\|}$  and  $\text{ME}_{\|q\|}$  by at least 28 and 60 times, respectively.
- Over the INIT maneuver, the KPIs measuring the position tracking performance (i.e.,  $\text{RMSE}_{\|q\|}$  and  $\text{ME}_{\|q\|}$  with  $\ell = \{q, p\}$ ) provided by the ROBUST-FL and PI-FL controllers are smaller than those obtained with the adaptive solutions. The reduced tracking performance of the adaptive solutions along the first submaneuver is due to the zero initialization of the adaptive gains, which generates larger initial errors over the first 35 s, referred to as  $t^*$  in the remainder (see also Figures 4A and 5A), and results in larger KPIs when the INIT maneuver is completed. The effect of the zero initialization on the KPIs is more severe for the EMRAC-NFL strategies, which, compared to the EMRAC-FL, are not equipped with the nominal FL control action.
- When the INIT maneuver is completed, the EMRAC adaptive gains have been self-adjusted to the actual plant dynamics, thus the residual tracking error and consequently the KPIs measuring the tracking performance shrink drastically. Furthermore, for the remaining submaneuvers (i.e., first-STST, first/second-LAP, second-STST), the KPIs measuring the tracking performance provided by the EMRAC solutions are always smaller compared to those obtained with the benchmark controllers (the ROBUST-FL strategy and the PI-FL controller). For instance, compared to the ROBUST-FL strategy, the EMRAC strategies reduce the  $\text{RMSE}_{\|p\|}$  by a factor that ranges (i) from 2.8 to 8.9 times in the case of the first-LAP maneuver, and (ii) from 5.2 to about 10 times over the second-LAP. Similarly, when compared to the PI-FL controller, the EMRAC strategies reduce the  $\text{RMSE}_{\|p\|}$  of a factor that ranges (i) from 2.6 to 8 times over the first-LAP maneuver, and (ii) from to 8.6 to 16.2 times over the second-LAP maneuver. A similar trend can be noted when comparing the KPIs tracking performance in the joint space of the adaptive solutions to those of the PI-FL and ROBUST-FL strategies over the first-LAP and second-LAP.

**TABLE 3** Performance indicators computed in the joint space (RMSE<sub>||q||</sub> (rad), RMSE<sub>||q̇||</sub> (rad/s), ME<sub>||q||</sub> (rad), ME<sub>||q̇||</sub> (rad/s), I<sub>||τ||</sub> (Nm), M<sub>||τ||</sub> (Nm)).

		EMRAC controllers				Benchmark controllers			
		EW-FL	EW-NFL	UV-FL	UV-NFL	ROBUST-FL	PI-FL	PD-FL	ROS-PID
INIT	RMSE <sub>  q  </sub>	1.58e-02	1.91e-02	8.36e-03	3.04e-02	9.19e-03	1.01e-02	1.32e-01	5.13e-02
	RMSE <sub>  q̇  </sub>	2.20e-03	2.65e-03	1.17e-03	4.34e-03	8.40e-04	9.57e-03	1.06e-02	1.20e-02
	ME <sub>  q  </sub>	3.55e-02	4.23e-02	1.82e-02	7.04e-02	1.46e-02	2.52e-02	2.72e-01	9.81e-02
	ME <sub>  q̇  </sub>	4.57e-03	6.48e-03	2.64e-03	9.26e-03	1.41e-03	2.59e-02	1.79e-02	2.22e-02
	I <sub>  τ  </sub>	2.46e+01	1.94e+01	2.34e+01	2.00e+01	1.67e+01	2.64e+01	1.28e+01	4.51e+01
	M <sub>  τ  </sub>	6.29e+01	4.56e+01	6.43e+01	7.03e+01	3.33e+01	5.59e+01	2.24e+01	9.78e+01
First-STST	RMSE <sub>  q  </sub>	9.18e-04	3.17e-03	1.21e-03	4.06e-03	7.82e-03	8.59e-03	2.87e-01	5.06e-02
	RMSE <sub>  q̇  </sub>	3.05e-04	1.51e-04	1.98e-04	2.43e-04	1.16e-03	4.99e-03	7.13e-03	1.45e-02
	ME <sub>  q  </sub>	1.17e-03	3.29e-03	1.42e-03	4.35e-03	1.07e-02	9.29e-03	3.03e-01	6.13e-02
	ME <sub>  q̇  </sub>	4.24e-04	2.55e-04	3.11e-04	3.20e-04	1.24e-03	5.99e-03	7.29e-03	2.11e-02
	I <sub>  τ  </sub>	1.31e+01	3.51e+00	1.30e+01	1.79e+00	2.87e+00	2.15e+01	3.66e+00	3.78e+01
	M <sub>  τ  </sub>	1.43e+01	4.14e+00	1.51e+01	2.03e+00	3.28e+00	3.04e+01	4.00e+00	6.05e+01
First-LAP	RMSE <sub>  q  </sub>	9.78e-03	1.84e-03	6.23e-03	2.68e-03	3.25e-02	2.59e-02	6.21e-01	4.46e-02
	RMSE <sub>  q̇  </sub>	1.85e-03	3.92e-04	1.13e-03	4.88e-04	4.05e-03	1.58e-02	1.27e+00	2.17e-01
	ME <sub>  q  </sub>	2.83e-02	4.11e-03	2.01e-02	6.32e-03	9.38e-02	6.20e-02	7.33e+00	1.24e-01
	ME <sub>  q̇  </sub>	5.62e-03	1.53e-03	3.78e-03	1.88e-03	1.14e-02	3.51e-02	1.52e+01	7.23e+00
	I <sub>  τ  </sub>	2.71e+01	2.33e+01	2.79e+01	2.27e+01	2.14e+01	4.07e+01	8.96e+02	1.34e+02
	M <sub>  τ  </sub>	1.09e+02	1.04e+02	1.05e+02	1.05e+02	1.05e+02	1.19e+02	2.00e+05	4.58e+03
Second-LAP	RMSE <sub>  q  </sub>	8.56e-03	2.28e-03	5.95e-03	2.91e-03	3.82e-02	5.30e-02		
	RMSE <sub>  q̇  </sub>	1.05e-03	3.73e-04	6.87e-04	5.22e-04	3.93e-03	3.31e-02		
	ME <sub>  q  </sub>	2.08e-02	5.80e-03	1.54e-02	8.57e-03	9.76e-02	9.93e-02		
	ME <sub>  q̇  </sub>	3.27e-03	9.38e-04	2.23e-03	1.93e-03	8.87e-03	6.72e-02		
	I <sub>  τ  </sub>	2.17e+01	2.22e+01	2.29e+01	2.17e+01	2.13e+01	7.19e+01		
	M <sub>  τ  </sub>	5.27e+01	5.48e+01	5.70e+01	5.34e+01	5.66e+01	1.34e+02		
Second-STST	RMSE <sub>  q  </sub>	1.81e-04	1.78e-04	3.34e-04	2.22e-04	4.74e-03	5.63e-02		
	RMSE <sub>  q̇  </sub>	3.18e-05	1.75e-05	1.41e-04	1.42e-05	2.89e-04	3.53e-02		
	ME <sub>  q  </sub>	2.15e-04	1.85e-04	4.49e-04	2.41e-04	5.40e-03	7.22e-02		
	ME <sub>  q̇  </sub>	5.07e-05	3.09e-05	3.00e-04	1.92e-05	3.35e-04	4.50e-02		
	I <sub>  τ  </sub>	5.99e+00	3.67e+00	6.05e+00	1.26e+00	1.28e+00	9.05e+01		
	M <sub>  τ  </sub>	6.23e+00	3.83e+00	7.10e+00	1.34e+00	1.47e+00	1.36e+02		

- Over the last maneuver (i.e, the second-STST maneuver), the tracking performance of the EMRAC solutions outperforms those of the ROBUST-FL algorithm even more. For instance, the EMRAC strategies reduce the RMSE<sub>||q||</sub> by a factor ranging from 14.2 to 26.2 times. Moreover, the ME<sub>||p||</sub> reduces by a factor that ranges from 11.5 to 27 times.
- For the PI-FL strategy, the RMSE<sub>||ℓ||</sub> indicators, with  $\ell = \{p, \dot{p}, q, \dot{q}\}$ , have an increasing trend over the last four maneuvers, which might mark the onset of unstable dynamics. For the ROBUST-FL algorithm, the magnitude of the KPIs measuring the tracking performance mainly depends on the trajectory to follow (e.g., the RMSE<sub>||ℓ||</sub>, with  $\ell = \{p, q\}$ , for the maneuver first-STST and second-STST are similar). However, for the EMRAC solutions, the mag-

TABLE 4 Performance indicators computed in the operational space ( $RMSE_{\|p\|}$  (m),  $RMSE_{\|\dot{p}\|}$  (m/s),  $ME_{\|p\|}$  (m),  $ME_{\|\dot{p}\|}$  (m/s)).

		EMRAC controllers				Benchmark controllers			
		EW-FL	EW-NFL	UV-FL	UV-NFL	ROBUST-FL	PI-FL	PD-FL	ROS-PID
INIT	$RMSE_{\ p\ }$	1.20e-01	1.34e-01	6.41e-02	2.33e-01	5.03e-02	3.19e-02	5.14e-01	3.56e-01
	$RMSE_{\ \dot{p}\ }$	1.64e-02	1.82e-02	8.40e-03	3.18e-02	4.59e-03	2.72e-02	4.60e-02	7.71e-02
	$ME_{\ p\ }$	2.71e-01	2.98e-01	1.45e-01	5.45e-01	7.96e-02	5.57e-02	1.08e+00	6.46e-01
	$ME_{\ \dot{p}\ }$	3.58e-02	4.33e-02	2.06e-02	6.45e-02	8.41e-03	5.94e-02	7.26e-02	1.31e-01
First-STST	$RMSE_{\ p\ }$	4.97e-03	1.69e-02	5.13e-03	2.16e-02	3.74e-02	4.05e-02	1.19e+00	2.67e-01
	$RMSE_{\ \dot{p}\ }$	1.59e-03	6.80e-04	9.77e-04	1.23e-03	5.87e-03	2.31e-02	4.39e-02	8.00e-02
	$ME_{\ p\ }$	6.30e-03	1.75e-02	6.19e-03	2.30e-02	5.21e-02	5.21e-02	1.29e+00	3.23e-01
	$ME_{\ \dot{p}\ }$	2.20e-03	1.00e-03	1.59e-03	1.41e-03	6.28e-03	3.03e-02	4.62e-02	1.12e-01
First-LAP	$RMSE_{\ p\ }$	3.07e-02	9.71e-03	2.10e-02	1.24e-02	8.68e-02	7.91e-02	1.92e+00	2.93e-01
	$RMSE_{\ \dot{p}\ }$	5.89e-03	1.56e-03	3.46e-03	1.97e-03	1.15e-02	4.47e-02	3.63e+00	4.29e+00
	$ME_{\ p\ }$	9.96e-02	1.85e-02	7.24e-02	2.28e-02	2.54e-01	1.63e-01	9.30e+00	1.93e+00
	$ME_{\ \dot{p}\ }$	2.03e-02	4.33e-03	1.31e-02	6.43e-03	3.75e-02	9.45e-02	3.65e+01	1.01e+02
Second-LAP	$RMSE_{\ p\ }$	2.21e-02	1.18e-02	1.49e-02	1.59e-02	1.15e-01	1.91e-01		
	$RMSE_{\ \dot{p}\ }$	3.33e-03	2.19e-03	2.53e-03	3.45e-03	1.06e-02	1.17e-01		
	$ME_{\ p\ }$	4.91e-02	2.66e-02	4.92e-02	4.32e-02	2.66e-01	3.21e-01		
	$ME_{\ \dot{p}\ }$	1.37e-02	6.27e-03	6.69e-03	1.41e-02	2.13e-02	1.93e-01		
Second-STST	$RMSE_{\ p\ }$	9.25e-04	6.42e-04	1.23e-03	8.44e-04	1.68e-02	2.47e-01		
	$RMSE_{\ \dot{p}\ }$	1.63e-04	8.02e-05	6.42e-04	5.17e-05	9.27e-04	1.56e-01		
	$ME_{\ p\ }$	1.10e-03	6.77e-04	1.59e-03	8.82e-04	1.83e-02	3.33e-01		
	$ME_{\ \dot{p}\ }$	2.65e-04	1.61e-04	1.24e-03	6.61e-05	1.05e-03	2.06e-01		

nitude of the KPIs could decrease for the same maneuver, because of the adaptation process.<sup>12</sup> For this case study, the reduction of the tracking errors caused by the gain adaptation is significant for the STST maneuvers. For instance, when second-STST is compared to first-STST, the  $RMSE_{\|p\|}$  reduces by 5.4 times and 25.6 times for the EMRAC-EW-FL and the EMRAC-UV-NFL, respectively.

- The KPIs measuring the control effort (i.e.,  $I_{\|\tau\|}$  and  $M_{\|\tau\|}$ ) show that the magnitude of the control action required by the EMRAC strategies matches the one demanded by the benchmark controllers that complete the entire maneuver (i.e., the ROBUST-FL controller and the PI-FL strategy).

## 6 | CONCLUSIONS

This paper has presented two extensions of the EMRAC strategy to multi-input plants. The novel multi-input EMRAC strategies, named EMRAC-UV and EMRAC-EW, include the  $\sigma$ -modification strategy to systematically bound all the adaptive gains also for not vanishing perturbations, but differ based on how the adaptive switching control action is computed. For both strategies, a proof of the global uniform ultimate boundedness of the closed-loop error dynamics has been derived, based on the Lyapunov theory for Filippov systems. The effectiveness of the multi-input EMRAC control framework has been numerically evaluated by designing and implementing, in a ROS-based simulation environment, four EMRAC solutions for controlling space robotic manipulators during the postcapturing phase, in case of unknown and noncooperative targets without any initial knowledge of the operating conditions. The simulation analysis has confirmed the ability of the adaptive closed-loop system to adjust to the unknown working conditions, thus providing low residual tracking errors. The EMRAC solutions have been compared with four benchmark controllers, that is, an embedded ROS PID controller, and PD, PI and robust controllers equipped with a full-state FL strategy. An extensive quantitative



analysis carried out through the use of KPIs defined in the joint space and operational space has confirmed that the closed-loop tracking performance of the EMRAC solutions outperforms those of the benchmark controllers after an initialization maneuver. Future work will investigate the experimental assessment of the proposed multi-input EMRAC schemes.

## CONFLICT OF INTEREST STATEMENT

We confirm that no one on the author list has a conflict of interest to disclose.

## DATA AVAILABILITY STATEMENT

Data available upon request to the authors.

## ORCID

Umberto Montanaro  <https://orcid.org/0000-0003-0620-1906>

## REFERENCES

1. Landau ID, Lozano R, Saad MM, Karimi A. *Adaptive Control: Algorithms, Analysis and Applications*. Springer-Verlag; 2011.
2. Nguyen NT. *Model-Reference Adaptive Control: A Primer*. Springer; 2018.
3. Torki W, Grouz F, Sbata L. A sliding mode model reference adaptive control of PMSG wind turbine. Paper presented at: International Conference on Green Energy Conversion Systems. Hammamet, Tunisia; 2017:1-6.
4. Jingzhuo S, Huang W. Model Reference Adaptive Iterative Learning Speed Control for Ultrasonic Motor. *IEEE Access*. 2020;8:181815-181824.
5. Baidya D, Roy R. *Speed Control of DC Motor Using Fuzzy-Based Intelligent Model Reference Adaptive Control Scheme. Lecture Notes in Electrical Engineering*. Vol 462. Springer; 2018:729-735.
6. Wei Y, Sun Z, Hu Y, Wang Y. On fractional order composite model reference adaptive control. *Int J Syst Sci*. 2016;47(11):2521-2531.
7. Xie J, Li S, Yan H, Yang D. Model reference adaptive control for switched linear systems using switched multiple models control strategy. *J Franklin Inst*. 2019;356(5):2645-2667. doi:10.1016/j.jfranklin.2018.10.036
8. di Bernardo M, Montanaro U, Santini S. Novel hybrid MRAC-LQ control schemes: synthesis, analysis and applications. *Int J Control*. 2008;81(6):940-961.
9. Xie J, Zhao J.  $H_\infty$  model reference adaptive control for switched systems based on the switched closed-loop reference model. *Nonlinear Anal Hybrid Syst*. 2018;27:92-106.
10. di Bernardo M, Montanaro U, Ortega R, Santini S. Extended hybrid model reference adaptive control of piecewise affine systems. *Nonlinear Anal Hybrid Syst*. 2016;21:11-21.
11. di Bernardo M, Hoyos Velasco CI, Montanaro U, Santini S. Experimental implementation and validation of a novel minimal control synthesis adaptive controller for continuous bimodal piecewise affine systems. *Control Eng Pract*. 2012;20(3):269-281.
12. di Bernardo M, di Gaeta A, Montanaro U, Santini S. Synthesis and experimental validation of the novel LQ-NEMCSI adaptive strategy on an electronic throttle valve. *IEEE Trans Control Syst Technol*. 2010;18(6):1325-1337.
13. Buonomano A, Montanaro U, Palombo A, Santini S. Building temperature control using an enhanced MRAC approach. Paper presented at: 2015 European Control Conference (ECC); IEEE; 2015:3629-3634.
14. Montanaro U, Gaeta d A, Giglio V. An MRAC approach for tracking and ripple attenuation of the common rail pressure for GDI engines. *IFAC Proc Vol*. 2011;44(1):4173-4180.
15. Buonomano A, Montanaro U, Palombo A, Santini S. Temperature and humidity adaptive control in multi-enclosed thermal zones under unexpected external disturbances. *Energy Build*. 2017;135:263-285.
16. Dixit S, Montanaro U, Dianati M, Mouzakitis A, Fallah S. Integral MRAC with bounded switching gain for vehicle lateral tracking. *IEEE Trans Control Syst Technol*. 2021;29:1936-1951.
17. Montanaro U, Gaeta d A, Giglio V. Robust discrete-time MRAC with minimal controller synthesis of an electronic throttle body. *IEEE/ASME Trans Mechatron*. 2014;19(2):524-537. doi:10.1109/TMECH.2013.2247614
18. Tao G. *Adaptive Control Design and Analysis*. John Wiley & Sons; 2003.
19. Khalil HK. *Nonlinear systems*. 2nd ed. Prentice Hall; 2002.
20. Mu XW, Ding ZS, Cheng GF. Uniformly ultimate boundedness for discontinuous systems with time-delay. *Appl Math Mech*. 2011;32(9):1187-1196.
21. Moosavian SAA, Papadopoulos E. Free-flying robots in space: an overview of dynamics modeling, planning and control. *Robotica*. 2007;25(5):537.
22. Wilde M, Choon SK, Grompone A, Romano M. Equations of motion of free-floating spacecraft-manipulator systems: an engineer's tutorial. *Front Robot AI*. 2018;5:41.
23. Flores-Abad A, Ma O, Pham K, Ulrich S. A review of space robotics technologies for on-orbit servicing. *Progr Aerospace Sci*. 2014;68:1-26.
24. Dubowsky S, Papadopoulos E. The kinematics, dynamics, and control of free-flying and free-floating space robotic systems. *IEEE Trans Robot Automat*. 1993;9(5):531-543.

25. Yoshida K, Nakanishi H, Ueno H, Inaba N, Nishimaki T, Oda M. Dynamics, control and impedance matching for robotic capture of a non-cooperative satellite. *Adv Robot.* 2004;18(2):175-198.
26. Shan M, Guo J, Gill E. Review and comparison of active space debris capturing and removal methods. *Progr Aerospace Sci.* 2016;80:18-32.
27. Yoshida K. Achievements in space robotics. *IEEE Robot Automat Mag.* 2009;16(4):20-28.
28. Virgili-Llop J, Zagaris C, Park H, Zappulla R, Romano M. Experimental evaluation of model predictive control and inverse dynamics control for spacecraft proximity and docking maneuvers. *CEAS Space J.* 2018;10(1):37-49.
29. Zhang X, Kamgarpour M, Georghiou A, Goulart P, Lygeros J. Robust optimal control with adjustable uncertainty sets. *Automatica.* 2017;75:249-259.
30. Huang P, Wang M, Meng Z, Zhang F, Liu Z, Chang H. Reconfigurable spacecraft attitude takeover control in post-capture of target by space manipulators. *J Franklin Inst.* 2016;353(9):1985-2008.
31. Nguyen-Huynh TC, Sharf I. Adaptive reactionless motion and parameter identification in postcapture of space debris. *J Guid Control Dynam.* 2013;36(2):404-414.
32. Stoten DP, Benchoubane H. Robustness of a minimal controller synthesis algorithm. *Int J Control.* 1990;51:851-861.
33. Buonomano A, Montanaro U, Palombo A, Santini S. Dynamic building energy performance analysis: a new adaptive control strategy for stringent thermohygrometric indoor air requirements. *Appl Energy.* 2016;163:361-386.
34. Montanaro U, Olm JM. Integral MRAC with minimal controller synthesis and bounded adaptive gains: the continuous-time case. *J Franklin Inst.* 2016;353(18):5040-5067.
35. Landau YD. *Adaptive Control: The Model Reference Approach.* CRC Press; 1979.
36. Miranda-Villatoro FA, Brogliato B, Castanos F. Set-valued sliding-mode control of uncertain linear systems: continuous and discrete-time analysis. *SIAM J Control Optim.* 2018;56:1756-1793.
37. Nakakuki T, Shen T, Tamura K. Adaptive control design for a class of nonsmooth nonlinear systems with matched and linearly parameterized uncertainty. *Int J Robust Nonlinear Control.* 2009;19:243-255.
38. Carignan C, Akin D. The reaction stabilization of on-orbit robots. *IEEE Control Sys Mag.* 2000;20(6):19-33. doi:10.1109/37.887446
39. Xu W, Liang B, Xu Y. Survey of modeling, planning, and ground verification of space robotic systems. *Acta Astronaut.* 2011;68(11):1629-1649. doi:10.1016/j.actaastro.2010.12.004
40. Wertz J, Everett D, Puschell J. *Space Mission Engineering: The New SMAD.* Space Technology Library, Microcosm Press; 2011.
41. Tummala AR, Dutta A. An overview of cube-satellite propulsion technologies and trends. *Aerospace.* 2017;4(4):58. doi:10.3390/aerospace4040058
42. Ketsdever AD, Micci MM. *Micropropulsion for Small Spacecraft.* American Institute of Aeronautics and Astronautics; 2000.
43. Siciliano B, Sciavicco L, Villani L, Oriolo G. *Robotics: Modelling, Planning and Control.* Springer; 2009.
44. Spong M. On the robust control of robot manipulators. *IEEE Trans Automat Control.* 1992;37(11):1782-1786.
45. Montanaro U, Costa-Castelló R, Olm JM, Barros CL. Experimental validation of a continuous-time MCSI algorithm with bounded adaptive gains. *J Franklin Inst.* 2019;356(12):5881-5897. doi:10.1016/j.jfranklin.2019.03.012
46. Shevitz D, Paden B. Lyapunov stability theory of nonsmooth systems. *IEEE Trans Automat Control.* 1994;39(9):1910-1914.
47. Cortes J. Discontinuous dynamical systems. *IEEE Control Syst Mag.* 2008;28(3):36-73.
48. Clarke FH. *Optimization and Nonsmooth Analysis.* Vol 5. SIAM; 1990.
49. gazebosim.org. Tutorial: Using Gazebo plugins with ROS. 2014. [http://gazebosim.org/tutorials?tut=ros\\_gzplugins](http://gazebosim.org/tutorials?tut=ros_gzplugins).
50. gazebosim.org. Tutorial: ROS communication. 2014. [http://gazebosim.org/tutorials/?tut=ros\\_comm](http://gazebosim.org/tutorials/?tut=ros_comm).
51. MathWorks. ROS toolbox. 2021. <https://uk.mathworks.com/help/ros>.

**How to cite this article:** Montanaro U, Martini S, Hao Z, Gao Y, Sorniotti A. Multi-input enhanced model reference adaptive control strategies and their application to space robotic manipulators. *Int J Robust Nonlinear Control.* 2023;33(10):5246-5272. doi: 10.1002/rnc.6639

## APPENDIX A. ULTIMATE BOUNDEDNESS OF NON-SMOOTH DYNAMIC SYSTEMS

This appendix provides details about the theory of nonsmooth dynamic systems, which has been used to prove the ultimate boundedness of the closed-loop error system when the multi-input EMRAC solutions are used. The theory can be applied to nonsmooth time-varying systems of the form

$$\dot{\tilde{x}} = \mathfrak{F}(t, \tilde{x}), \quad (\text{A1})$$

where  $\tilde{x} \in \mathbb{R}^n$  is the state of the system and  $\mathfrak{F}: \mathbb{R} \times \mathbb{R}^n \rightarrow \mathbb{R}^n$  is a discontinuous vector field.

According to References 46,47, a vector function  $\tilde{x}(\cdot)$  is a Filippov solution of the discontinuous system (A1) for  $t \in [t_0, t_1]$  if (i)  $\tilde{x}(\cdot)$  is absolutely continuous, and (ii) for almost all  $t \in [t_0, t_1]$

$$\dot{\tilde{x}} \in \mathbf{K}[\mathcal{F}](t, \tilde{x}), \quad \text{with} \quad \mathbf{K}[\mathcal{F}](t, \tilde{x}) \triangleq \bigcap_{v>0} \bigcap_{\pi(S)=0} \text{co} \{ \mathcal{F}(t, \mathcal{B}(\tilde{x}, v) \setminus S) \}, \quad \tilde{x} \in \mathbb{R}^n, \quad (\text{A2})$$

where  $\mathbf{K}[\mathcal{F}]$  is the Filippov set valued map,  $\bigcap_{\pi(S)=0}$  denotes the intersection of all sets  $S$  of Lebesgue measuring zero,  $\overline{\text{co}}$  is the convex closure, and  $\mathcal{B}(\tilde{x}, v)$  is the open ball centered at  $\tilde{x}$  with radius  $v > 0$ . Furthermore, according to theorem 2.2 in Reference 46, given a Lipschitz regular function  $V : \mathbb{R}^+ \times \mathbb{R}^n \rightarrow \mathbb{R}$ , then the function  $V(t, \tilde{x}(t))$  is absolute continuous along the Filippov solutions of system (A2),  $\frac{d}{dt}V(t, \tilde{x}(t))$  exists almost everywhere and

$$\frac{d}{dt}V(t, \tilde{x}(t)) \in^{\text{a.e.}} \dot{V}(t, \tilde{x}(t)), \quad (\text{A3})$$

where the set-valued map  $\dot{V}$  is computed as

$$\dot{V} = \bigcap_{\xi \in \partial V(t, \tilde{x})} \xi^T \begin{pmatrix} \mathbf{K}[\mathcal{F}](t, \tilde{x}) \\ 1 \end{pmatrix}, \quad \text{with} \quad \partial V(t, \tilde{x}) = \overline{\text{co}} \{ \lim \nabla V(t, \tilde{x}) | (t_i, \tilde{x}_i) \rightarrow (t, \tilde{x}), (t_i, \tilde{x}_i) \notin \Xi_V \} \quad (\text{A4})$$

where  $\partial V(t, \tilde{x})$  is the Clarke's generalized gradient,<sup>48</sup> and  $\Xi_V$  is the set of measure zero where the gradient of  $V$  is not defined. Furthermore, according to Reference 46, when  $V$  is a smooth function (i.e., a differentiable function) with respect to  $\tilde{x}$  and does not depend on time, (A4) reduces to

$$\dot{V}(t, \tilde{x}(t)) = \nabla V^T \cdot \mathbf{K}[\mathcal{F}](t, \tilde{x}). \quad (\text{A5})$$

Similarly to the case of smooth dynamic systems,<sup>19</sup> the solutions of system (A1) are said to be uniformly ultimately bounded with ultimate bound  $\epsilon_{ub} > 0$  if there exists a time interval  $\mathcal{T}$  (dependent on  $\tilde{x}(t_0)$ ) and a  $\mathcal{KL}$ -function  $\Psi : \mathbb{R}^+ \times \mathbb{R}^+ \rightarrow \mathbb{R}^+$  such that

$$\|\tilde{x}(t)\| \leq \Psi(\tilde{x}(t_0), t - t_0), \quad \forall t_0 \leq t \leq t_0 + \mathcal{T}, \quad \text{and} \quad \|\tilde{x}(t)\| \leq \epsilon_{ub}, \quad \forall t \geq t_0 + \mathcal{T}. \quad (\text{A6})$$

Unfortunately, the theory presented in Reference 19 cannot be used to system (A1), as it assumes a locally Lipschitz vector field. However, the conditions for guaranteeing the ultimate boundedness have been recently extended to nonsmooth systems in Reference 20, and the main result is summarized below.

**Theorem 3.** *Assume that the differential inclusion (A2) is well-posed in the sense of Filippov solutions for any initial condition, and there exists a positive globally Lipschitz continuous function  $V : \mathbb{R}^+ \times \mathbb{R}^n \rightarrow \mathbb{R}$ , two positive functions  $W_1, W_2 \in \mathcal{K}_\infty$ , a positive function  $W_3 \in \mathcal{K}$  and a constant  $\mu > 0$  such that*

$$W_1(\tilde{x}) \leq V(t, \tilde{x}) \leq W_2(\tilde{x}), \quad \text{and} \quad \dot{V}(t, \tilde{x}) \leq -W_3(\tilde{x}) \quad \forall \|\tilde{x}\| \geq \mu. \quad (\text{A7})$$

*Then the nonsmooth system (A1) is globally uniformly ultimately bounded and the ultimate bound is given by  $W_1^{-1}(W_2(\mu))$ .*

Theorem 3 is a special case of theorem 3.1 in Reference 20 by assuming (i) absence of time delays, (ii) the existence of the solution of the differential inclusion (A2) for any initial condition, and (iii) definition of  $V(t, \tilde{x})$  over the entire  $\mathbb{R}^n$ .

## APPENDIX B. SIMULATION ENVIRONMENT AND DEPLOYMENT OF CONTROLLERS IN ROS

The multiplatform simulation framework used for testing the EMRAC solutions and the benchmark controllers in Section 5 consists of (i) ROS, which is widely used for various real time robotic applications; (ii) *Gazebo*, which is a three-dimensional multirobot simulator and includes the C-based Open Dynamics Engine for simulating rigid body dynamics; and (iii) *MatLab/Simulink* with build-in *ROS Toolbox* which interfaces MatLab/Simulink and ROS, and

supports C++ code generation. The simulation framework is completed with two *ad hoc* in-house C++ and Python codes whose uses are detailed below.

The robotic arm within the simulator is modeled through the Unified Robotic Description (URDF) format. The micro-satellite attached to the end-effector is modeled in the URDF file as an additional fixed link. A picture of Gazebo when the URDF is loaded is shown in Figure 1.

The non-cooperative target disturbance in (69) is emulated by using the *IMU plugin sensor*,<sup>49</sup> the *apply\_body\_wrench* service,<sup>50</sup> and the in-house Python script. The IMU plugin is a build-in feature provided in Gazebo. It measures and publishes the acceleration information of a selected 'link'. In the simulation, the IMU plugin is added to the target. The in-house Python script is used to subscribe the acceleration information of the target and subsequently calculate the reaction forces generated by the target in (69). Then the *apply\_body\_wrench* ROS service<sup>50</sup> is recalled to apply the attitude disturbance forces to the target.

The four EMRAC solutions and the benchmark controllers (except for the ROS-PID controller) in Sections 4 and 5 are implemented in Matlab/Simulink and connected to the ROS environment through the ROS Publish and Subscribe blocks (available in the MatLab ROS toolbox). The Publish block uses the node of the Simulink model to create a ROS publisher for a specific topic. The input of this block is a Simulink nonvirtual bus that corresponds to the specified ROS message type and publishes it to the ROS network. For the specific simulation framework, one Publish block was used for each of the three joint torques, creating the topics named `/space_arm/joint_i_position_controller/command` ( $i = 1, 2, 3$ ) and providing the torque values (computed by the controller) using the `std_msgs/Float64` message type. The block is responsible for converting the Msg input from a Simulink bus signal to a ROS message and publishing it at each sampling time. In code generation, the input is a C++ ROS message.<sup>51</sup> The Subscribe block uses the Simulink model node to create a ROS subscriber for a specific topic, takes a specified ROS message type as input, and provides a corresponding Simulink nonvirtual bus as output. The URDF model publishes the joint states values to the `/space_arm/joint_states` topic using `sensor_msgs/JointState` message type, thus, a Subscribe block was used to feed the manipulator's joint position and velocities to the controller. The block is responsible, on each simulation step, for checking if a new message is available on the specific topic and, if it is, retrieving the message and converting it to a Simulink bus signal.<sup>51</sup> The combined use of these two blocks allows for providing the controller output torques to the URDF manipulator which, in return, feeds the joint states signals to the control algorithm, therefore enabling to close the control loop. An additional "To File" block is added in the Simulink model in order to collect all the simulation data and store them into a MAT-file. The "To File" block is compatible with C++ code generation and has minimal memory overhead during simulation, which means that it will not affect the performance of the controller.

The Simulink code of each controller is converted into a C++ code by using Simulink Coder and Embedded Coder. Furthermore, to finalize the deployment of the code of the controller into the simulation framework, the in-house C++ code has been developed which subscribes to the `/space_arm/joint_i_position_controller/command` topic and applies the controller' input torques values to the URDF manipulator joints using the *EffortJointInterface* hardware interface. Finally, after the simulations in Gazebo, a MAT-file with all the simulation data will be created.